Gondwana break-up related magmatism in the Falkland Islands

Journal Item

Gondwana break-up related magmatism in the Falkland Islands

M. J. Hole[1], R.M. Ellam[2], D.I.M. MacDonald[1] & S.P. Kelley[3]

[1] *Department of Geology & Petroleum Geology University of Aberdeen, AB24 3UE, UK*
[2] *Scottish Universities Environment Research Centre, East Kilbride, Glasgow, G75 0QU, UK*
[3] *Department of Earth & Environmental Sciences, Open University, Milton Keynes, MK7 6AA UK*

Jurassic dykes (178-182 Ma) are widespread across the Falkland Islands and four distinct suites of intrusions are recognized. NW-SE oriented dykes have εNd_{182} in the range -6 to -11 and $^{87}Sr/^{86}Sr_{182}$ >0.710 and therefore require an old lithospheric component in their source. Major element variations show that these intrusions were probably derived from a pyroxenite-rich source. A suite of basaltic-andesites and andesites exhibit major and trace element compositions that are similar to Ferrar dolerites, but they have εNd_{182} c. 0 and $^{87}Sr/^{86}Sr_{182}$ <0.7055 showing that they were derived from a less isotopically enriched source than the Ferrar dolerites. Basalt intrusions with $^{87}Sr/^{86}Sr_{182}$ c. 0.7035 and εNd_{182} c. +4, and low Th/Ta and La/Ta ratios (c. 1 and c. 15 respectively) escaped interaction with the lithosphere, and represent syn-break-up, asthenosphere-derived magmas emplaced at the initiation of oceanic spreading. Magmatism occurred on the periphery of the plume system centred on Dronning Maud Land, but there is no evidence to suggest that mantle potential temperatures were more than 1450°C in the Falkland Islands, leading to the possibility that melting occurred by decompression of mantle that had undergone internal heating whilst isolated beneath Gondwana for 100s of Ma.

The Early Jurassic (c. 180 Ma) Karoo and Ferrar large igneous provinces (LIP) were associated with Gondwana break-up. Two distinct geochemical associations of low TiO_2 continental flood basalts (CFB) have been identified on the basis of both their geochemical characteristics and geographical distribution. Igneous rocks of the Karoo province occur predominantly in South Africa but extend into Dronning Maud Land (Antarctica) with the main phase of activity taking place in the interval 178-184 Ma (Jourdan *et al.* 2004; 2005; 2007a; Riley *et al.* 2004). The Ferrar Province, which is contemporaneous with the magmatism in the Karoo province (Encarnacion *et al.* 1996; Fleming *et al.* 1997), is typified by the low TiO_2 Jurassic igneous rocks of the Transantarctic Mountains and Tasmania (Hergt *et al.* 1989; Fleming *et al.* 1995). It has also been established that the Karoo and Ferrar provinces have areas of geographical overlap, most notably in the KwaZulu area of South Africa (Riley *et al.* 2006; Sweeney *et al.* 1994) and in the Theron Mountains of Antarctica (Brewer *et al.* 1992). In the latter, at least four suites of low TiO_2 igneous rocks have been recognized, and it has been suggested that there is a transition from one province to the other rather, than a strict geographical delineation between the two provinces (Brewer *et al.* 1992). Hole (2015) argued that the melting to form the most magnesian Ferrar magmas required mantle potential temperatures (T_P) of c. 1450°C, around 100°C higher than ambient mantle (c. 1350±50°C) and consequently may have been generated by decompression melting of internally heated mantle melting being facilitated by Jurassic rifting. In this case there is no need for a mantle plume to generate Ferrar magmas. However, picritic magmatism in Dronning Maud Land, which was broadly synchronous with the emplacement of the Ferrar dolerites, required $T_P > 1550$°C, a temperature that is too high to be achieved by internal heating of the mantle and may therefore require the action of a hot mantle plume (Hole 2015; Coltice *et al.* 2009).

Elliott & Fleming (2000) argued that the focus of magmatism for both the Karoo and Ferrar provinces was the Weddell Triple Junction (WTJ; Fig. 1) which was within the envelope of a plume-related thermal anomaly associated with Gondwana break-up. Prior to Gondwana fragmentation, plate reconstructions place the Falkland Islands on the extension of the Cape Fold Belt of South Africa, on the eastern flank of the Lebombo Rift (Fig. 1; Macdonald *et al.* 2003; Stone *et al.* 2008; 2009; Richards *et al.* 2013). By about 180 Ma, the islands had undergone 90° of rotation and consequently had passed over the locus of the WTJ. By the early Cretaceous (c. 135 Ma), the Falkland Islands had rotated a further 90° and had migrated to the west along the extension of the Aghulas Fracture zone to a position well to the west of the WTJ.

Since the Falkland Islands may have been very close to the focus of break-up related magmatism, it is logical to assume that the geochemical composition of any igneous rocks found in the islands should reflect the diversity of magmatism in the Jurassic Gondwana LIP as a whole. In this paper, new data are presented that show that the dykes and minor intrusions of the Falkland Islands exhibit variability in mineralogy, major element, trace element and Sr-, Nd- and Pb-isotopic compositions that is nearly as large as that seen in the entire Jurassic Gondwana LIP, even though the Falkland Islands themselves represent an area of 400km^2 kilometres. Intrusions with major and trace element characteristics most similar the Ferrar dolerites of the Transantarctic Mountain are juxtaposed with intrusions which are nearly identical to some Karoo basalts of South Africa and Antarctica.

Falkland Islands Dyke Swarm

Dolerite dykes, mostly of Jurassic age, are widespread in West Falkland and rather sparse in East Falkland (Fig. 2; Greenway 1972; Mussett & Taylor 1994; Thistlewood *et al.* 1997; Mitchell *et al.* 1999; Stone *et al.* 2008, 2009; Richards *et al.* 2013). Distinct sub-swarms of dykes have been recognized based on azimuth of exposed intrusions and aeromagnetic anomalies (Mitchell *et al.* 1999; Stone *et al.* 2009). Prominent dolerite dykes, tens of metres wide and oriented NE-SW, are present in both West and East Falkland and are reversely magnetized. This suite corresponds to the N-S suite of Mitchell *et al.* (1999), and is of Jurassic age (c. 178-188 Ma; Mussett & Taylor 1994; Stone *et al.* 2009). E-W oriented olivine-dolerite dykes occur locally in the south of West Falkland, and they form part of a larger suite of intrusions that Stone *et al.* (2009) suggest has a partially radial disposition. In addition, Richards *et al.* (2013) noted that there is a suite of about 40, N-S oriented magnetic anomalies, that may represent intrusions, and these occur across the entire Falkland Islands. Exposed examples from Teal Creek and Peat Banks (Fig. 2) yield $^{40}Ar/^{39}Ar$ ages in the range 133-138 Ma and these dykes are likely to be members of the Etendeka suite of south-western Africa (Stone *et al.* 2009; Richards *et al.* 2013). During the current study, $^{40}Ar/^{39}Ar$ step-heating analysis was carried-out on separated plagioclase feldspar phenocrysts from three samples, but only one of these yielded useful information. Sample WI-5, a NE-SW oriented dyke from Weddell Island (Fig. 2), which is also within the area of the radial swarm identified by Richards *et al.* (2013), contains abundant plagioclase phenocrysts, and yielded a precise age of 182.3±1.5 Ma (Fig. 3). This confirms a Jurassic age for some of the Falkland Islands intrusions, and it is within error of the 178.6±4.9 Ma determined by Stone *et al.* (2008) for an aphyric NE-SW dyke from Port Sussex Creek, East Falkland (Fig. 2).

Selected major and trace element abundances *versus* weight % MgO for 139 intrusions from the Falkland Islands, including 109 from this study and 30 from Mitchell *et al.* (1999), are shown in Fig. 4 and representative analyses are given in Table 1. Mitchell *et al.* (1999) divided the intrusions of the Falkland Islands into two main N-S and E-W suites based on azimuth, field occurrence, petrography, mineral chemistry and whole-rock geochemical data. A subsidiary three magma types were also tentatively identified by Mitchell *et al.* (1999), including 'evolved N-S', Lively Island and Mount Alice types. The reassessment of the spatial distribution, orientation and age of the dyke swarms by Stone *et al.* (2009) and Richards *et al.* (2013), along with the much enlarged data set for the igneous rocks of the Falkland Islands generated for this study, now allows the identification of six individual geochemical types of intrusions. The criteria used to separate the different groups of intrusions are given in Table 2 and are illustrated in Figs 4 to 10. A description of each suite is given below.

Port Sussex Creek-type intrusions (PST). All the N-S dykes of Mitchell *et al.* (1999) are included in this suite of intrusions. PST intrusions are widely distributed across both East Falkland and West Falkland, all are sub-vertical with an azimuth of NE-SW, and they are consistently between 8 and 10 m in thickness. A typical example occurs at Port Sussex Creek, East Falkland, (MHF1; Table 1, Fig. 2), and is an 8m wide, sub-vertical, medium-grained, spheroidally-weathering dolerite dyke with an azimuth of 40º magnetic (NE-SW) and an age of 178.6±4.9Ma (Stone *et al.* 2008). The texture is equigranular and intersertal. Pyroxene is enstatite ($En_{70}Wo_4Fs_{26}$), pigeonite ($En_{51}Wo_{13}Fs_{36}$) and augite (Fig. 7) and the feldspar is labradorite (An_{70}). All PST intrusions contain both augite and pigeonite, with more mafic samples containing orthopyroxene. Olivine (Fo_{50-71}) is rare in this suite of rocks and is restricted to intrusions with Mg# >58 (e.g. FAR1503 and NGF16; Table 1, Fig. 4). Whole-rock MgO contents vary from 5.9-9.5 weight % (Mg# 50-62) and SiO_2 (53-55 weight %) is higher for a given MgO concentration than any of the other Falkland Islands intrusions (Fig. 4). The PST intrusions are characterized by low CaO (8.1-9.8 weight %) for a given MgO content compared to other Falkland Islands intrusions. TiO_2 abundances (0.9-1.2 weight %) are typical of the low TiO_2 Gondwana break-up related LIPs of the southern hemisphere (Fig. 6). Abundances of Cr are unusually high (up to 648 ppm) for samples with SiO_2 in their range, and are reflected in the high Cr content of orthopyroxene. Abundances of Nb and Y are restricted to 2-5 and 19-23 ppm respectively. PST intrusions are LREE enriched (Fig. 7) with $[La/Yb]_N$ in the range 3.2-3.9 and samples lack any significant Eu anomaly (Eu/Eu* 0.89-0.97). La/Ta and Th/Ta are the highest of any of the Falkland Islands samples analysed (44-52 and 5.9-8.6 respectively), and consequently, on ORB-normalized multi-element diagrams (Fig. 8), samples exhibit a marked trough in the abundances of Ta and Nb relative to Th, U, K and La (Fig. 9). $[Ta/Yb]_N$ is in the range 2.0 to 2.6, the lowest values for any of the Falkland Islands intrusions. Ti/Zr and P/Zr (55-60 and 4.5-6.3 respectively) are such that all PST intrusions exhibit a minor trough at Ti and P relative to adjacent elements on ORB-normalized diagrams. εNd_{180} varies from -5.5 to -11.0 and is accompanied by radiogenic Sr-isotopic compositions ($^{87}Sr/^{86}Sr_{180}$ 0.7070-0.7134), although Sr-Nd isotope covariations are rather scattered (Fig. 9). Pb-isotopic compositions form an array that is close to the Geochron ($^{207}Pb/^{204}Pb$ =15.55-15.65), and extends to $^{206}Pb/^{204}Pb$ ratios of up to 18.40. $^{207}Pb/^{204}Pb$ exhibits a negative correlation with εNd_{180} for PST intrusions (Fig. 9). Marked negative correlations between 1/Sr and $^{87}Sr/^{86}Sr_{182}$, εNd_{182} and Th/Ta and a positive correlation between MgO and εNd_{182} suggests that PST dykes underwent interaction with a high $^{87}Sr/^{86}Sr_{182}$ (> 0.714), low εNd_{182} (< -12) component that had Th/Ta > 9, and that interaction was concomitant with crystallization (Fig. 10).

E-W intrusions. A description of this type of intrusions is given by Mitchell *et al.* (1999). E-W intrusions are restricted to the central part of West Falkland (Fig. 2) and are generally medium-grained olivine-phyric dolerites (Fo_{82} at 11 weight % MgO in the whole-rock), the only pyroxene present being augite (Fig. 5). E-W intrusions are distinguished from the PST (Fig. 6) by their lower SiO_2 contents (48-52 weight %) and higher Ti/Zr (80-95) for a similar range in TiO_2, and MgO content (1.0-1.4 and 4.8-11.4 weight % respectively). E-W intrusions have $[La/Yb]_N$ in the range 2.1-4.0 (Fig. 7) and no appreciable Eu anomaly (Eu/Eu* 0.89-1.0). $[Ta/Yb]_N$ ratios are in the range 2.8 to 4.7, and all samples exhibit a negative Nb, Ta trough relative to the LILE (La/Ta, 16-27, Th/Ta 2.2-2.8) but this is not as pronounced as that for the PST intrusions. E-W intrusions have isotopic compositions that are close to, or slightly depleted relative to the Chondritic Uniform Reservoir (εNd_{180} = -0.4 to 3.0; $^{87}Sr/^{86}Sr_{180}$= 0.7036-0.7058) and have Pb-isotopic compositions that lie just above the NHRL (Fig. 9)

Lively Island intrusion. A single 30m thick intrusion which is exposed on Lively Island has noticeably lower TiO_2 for a given MgO content than any other of the Falklands Islands intrusions (TiO_2 = 0.8 weight % at 6 weight % MgO) and the data falls close to the compositional trend for low TiO_2 Ferrar dolerites from the Transantarctic Mountains (Fig. 6). Characteristic mineralogical features are the presence of sparse, Mg-rich biotite and rare Ca-poor groundmass pyroxene (Fig. 5). The intrusion has a LREE-enriched REE profile ($[La/Yb]_N$

= 3.2) which lacks a significant negative Eu anomaly (Eu/Eu* = 0.87). La/Ta and Th/Ta (20.4 and 3.2 respectively) are similar to E-W intrusions and considerably lower than for PST intrusions (Table 2). The Lively Island intrusion contains radiogenic Nd and unradiogenic Sr (εNd_{180} -0.5, $^{87}Sr/^{86}Sr_{180}$ c. 0.7060) compared to PST intrusions.

Dyke Island Type (DIT). The greatest concentration of DIT intrusions is on aptly-named Dyke Island (Fig. 2). In addition, the evolved N-S samples described by Mitchell *et al.* (1999) are of this type (e.g. NHF17; Fig. 2). Intrusions are generally <50 cm thick, they may contain abundant plagioclase ± augite phenocrysts (samples WI-5, MHF14.9 and FAR338), or more commonly they are medium- to fined-grained aphyric basaltic-andesites and andesites with rare rhyolite sheets occurring locally. DIT intrusions represent an expanded fractionation series with MgO varying from 5.6 to <0.1 weight %, over a range of 51-75 weight % SiO_2. Ti/Zr is in the range 32-55 for samples with 4.0-5.6 weight % MgO, and for samples with <1 weight % MgO, Ti/Zr falls to <5 (Fig. 6). All DIT intrusions have higher concentrations of the incompatible elements Zr, Nb and Y than any of the other intrusions from the Falkland Islands, and exhibit strong positive linear correlations between these elements. On a plot of TiO_2 *versus* MgO (Fig. 6) DIT intrusions can be divided into three distinct series; i) a low TiO_2 series which forms and extension of the data array for PST intrusions; ii) a high TiO_2 series with MgO in the range 2.5-4.0 weight % MgO with TiO_2 > 1.7 weight %; and iii) acid intrusions with < 2 weight % MgO.

DIT intrusions are LREE-enriched ($[La/Yb]_N$ = 4.1-6.6; Fig. 7) and exhibit stepwise increases in both LREE and HREE abundances with decreasing MgO with the most evolved sample (MHF41.3, 0.06 weight % MgO) having La_N = 290 and Yb_N = 44. The development of a progressively larger negative Eu anomaly (Eu/Eu* 0.85-0.71) with decreasing MgO, attests to the importance of plagioclase fractionation during their petrogenesis. Th/Ta and La/Ta for the DIT intrusions (2.4-3.4 and 17-26 respectively) are similar to those for the E-W intrusions. Multi-element diagrams (Fig. 8) show that DIT intrusions exhibit troughs at Ti and P relative to adjacent elements, and a progressively larger negative Sr anomaly is developed with decreasing MgO. Plagioclase-phyric samples WI-5 and FAR338 exhibit a positive Sr spike in Fig. 8, which is presumably a result of accumulation of plagioclase feldspar, although neither sample exhibits a Eu anomaly. The distribution of trace elements in DIT intrusions bears a strong resemblance to those for Ferrar dolerites from the Transantarctic Mountains (Fig. 8). DIT intrusions have $^{87}Sr/^{86}Sr_{180}$ in the range 0.7055-0.7170 but all samples with $^{87}Sr/^{86}Sr_{182}$ > 0.7090 contain < 2 weight % MgO. εNd_{182} falls in the range -2.8 to +0.6, and there is no systematic variation between MgO, εNd_{182} or $^{87}Sr/^{86}Sr_{182}$ (Figs 9 & 10).

Mount Alice Type intrusions (MAT). MAT intrusions are restricted to the south-western area of West Falkland, around South Harbour, Dyke Island and Cape Orford (Fig.1) and are early Jurassic in age (188±2 Ma for sample MA3; Mussett & Taylor 1994). MAT intrusions are generally < 1 m thick and are characterized by plagioclase ± augite ± olivine phenocrysts in a fine-grained groundmass. Since the area in which the MAT intrusions occur is within the region of the radial dyke swarm described Richards *et al.* (2013), azimuths cannot be used as one of their classification criteria, although in the region of Cape Orford, MAT dykes are generally oriented E-W (Mussett & Taylor 1994; Thistlewood *et al.* 1997). A typical example (MFH15.2) contains sparse, scattered phenocrysts of olivine (Fo_{80}), calcic augite ($En_{31}Fs_{25}Wo_{44}$; Fig. 5) and labradorite (An_{60}). MgO varies from 6-12 weight %, and the MAT intrusions have the lowest SiO_2 (46-50 weight %) for a given MgO content of any of the Falklands Islands samples (Fig. 4). TiO_2 abundances (1.3-2.0 weight %) overlap with those for both the PST and E-W intrusions but Ti/Zr is in the range 90-150 which is considerably higher than any other of the Falkland Islands intrusions. MAT intrusions have $[La/Yb]_N$ in the range 1.8-3.1 (Fig. 7) and flat to slightly LREE-depleted REE profiles for elements La to Sm ($[La/Sm]_N$ 0.9-1.5). On multi-element diagrams (Fig. 8), MAT intrusions exhibit a positive Sr spike relative to N-ORB, but otherwise have smooth profiles from elements Nd to Lu, with Ti/Zr and P/Zr (98-130 and 8.0-10.4 respectively) in the range for normal ORB (Ti/Zr c. 100, P/Zr c. 6.9; Sun & McDonough

1987). Unlike all the other Falkland Islands intrusions, the MAT have Th/Ta and La/Ta (0.7-1.0 and 13-17 respectively) which are also within the range for normal ocean ridge basalts and asthenosphere-derived basalts (Sun & McDonough 1987). Sr- & Nd-isotopic compositions fall in the upper-left quadrant of Fig. 10, with $\varepsilon Nd_{180} > 5$ and $^{87}Sr/^{86}Sr_{180} < 0.7040$. Pb-isotopic compositions fall just above the NHRL with $^{206}Pb/^{204}Pb$ in the range 18.2-18.5 (Fig. 9).

Provinciality of Falkland Islands intrusions

The Karoo and Ferrar LIPs can be separated from one another on the basis of MgO, SiO_2, TiO_2 content and Ti/Zr. These differences are illustrated in Fig. 6. The Ferrar LIP has two distinct lineages of igneous rocks one of which is typified by the low TiO_2 and low Ti/Zr basalts and basaltic-andesites of the Transantarctic Mountains and the other by the slightly higher TiO_2 series of the Theron Mountains (Fig. 5). Brewer *et al.* (1992) argued that the Theron Mountinas represented the geographical region of overlap of the Karoo and Ferrar LIPs. Ferrar LIP volcanic rocks have also been recognized in southern Africa (Riley *et al.* 2006) and so the geographical distribution of Ferrar LIP igneous rocks is not simple. Karoo LIP igneous rocks belong to a higher TiO_2 and lower SiO_2 suite than the Ferrar LIP. Within Dronning Maud Land, at least four component magma types of the Karoo LIP have been recognized (Fig. 5). These comprise chemical types CT1, CT2 and CT3 (Luttinen *et al.* 1998; Luttinen & Furnes (2000), plus the dolerites of the Kirwanveggan (Harris *et al.* 1990). There is a total overlap in the MgO, SiO_2, TiO_2 content and Ti/Zr of the Dronning Maud Land igneous rocks and those of South Africa (not shown).

Figure 6 shows that PST intrusions exhibit similar variations in MgO, TiO_2 and Ti/Zr to the low TiO_2 suite of the Theron Mountains (Brewer *et al.* 1992) and to CT1 basalts of Dronning Maud Land (Luttinen & Furnes 2000). However, the limited SiO_2 content of the PST intrusions suggests a stronger affinity with CT1 basalts than Theron Mountains samples, the latter of which have a much broader range in SiO_2 than CT1 and PST samples. Whilst E-W intrusions have ranges in MgO, SiO_2 and TiO_2 contents that are typical of Karoo LIP igneous rock, Ti/Zr ~80 and SiO_2 47-52 weight % are closest to the composition of basalts from Kirwanveggan and Schirmacher Oasis, Dronning Maud Land (Fig. 8; Harris *et al.* 1990; Sushchevskaya *et al.* 2009). DIT intrusions exhibit similar distributions in MgO and TiO_2 to basalts and basaltic-andesites from the Theron Mountains (Brewer *et al.* 1992) and Transantarctic Mountains (Fleming *et al.* 1995). Evolved (SiO_2 > 60 weight %) igneous rocks, similar to some of the DIT intrusions, have also been reported from the Transantarctic Mountains and Tasmania (Melluso *et al*. 2013). Characteristic features of intermediate compositions from the Transantarctic Mountains are troughs at Sr, Ti and P on multi-element diagrams (Fig. 8) which DIT samples with < 5 weight % MgO share. MAT intrusions have unusually high Ti/Zr (85-150) a characteristic that they share with CT2 and CT3 basalts of Dronning Maud Land and Rooi Rand ORB-like dykes (Melluso *et al*. 2008) from the Southern Lebombo of Africa (Fig. 6). Given that the data shown in Fig. 5 encompasses the entire compositional variability within the Karoo and Ferrar LIPs, it is striking that the majority of the low TiO_2 break-up related magma types are all represented within a small geographical area of the Falkland Islands. Indeed, within an area of 400km^2 centred on Dyke Island, magma types representing compositions similar to the CT1 and Kirwanveggan of Dronning Maud Land, the low and high TiO_2 dolerites of the Theron Mountains, and intermediate to acid compositions of the Transantarctic Mountains and Tasmania are all represented. The geographical boundaries of the Karoo and Ferrar LIPs therefore requires re-evaluation. Firstly the detailed petrogenetic history of the different groups of Falkand Islands intrusions will be considered.

Petrogenesis of the Falkland Islands intrusions

PST intrusions

PST and low TiO_2 DIT intrusions exhibit variations in major element compositions that fall along the same fractionation trend as low TiO_2 basaltic-andesites and andesites from the Theron Mountains (Figs. 5 & 6). However, PST and DIT intrusions cannot be related to one another by simple crystal fractionation because their Sr-, Nd- and Pb-isotopic compositions differ significantly from one another (Fig. 10). The high $^{87}Sr/^{86}Sr_{182}$ (> 0.710) and unradiogenic Nd-isotopic compositions of the PST is a feature they share with Ferrar dolerites. Fleming *et al.* (1995) and Molzhan *et al.* (1999) demonstrated that the relatively consistent εNd_{182} (-4.8 to -5.4), but highly variable $^{87}Sr/^{86}Sr_{182}$ (0.7090-0.7112) of the MFCT was partly a function of Rb and Sr mobility during a Cretaceous (97-125 Ma) hydrothermal event. This cannot be used as an explanation for variability in the Sr-isotopic compositions of PST intrusions because the Falkland Islands would have already broken-away from the Antarctic continent by this time. In addition, the range of εNd_{182} from -6 to -12 over the limited range of $^{87}Sr/^{86}Sr_{182}$ = 0.7110-0.7115, requires potential contaminants that had a range of Nd-isotopic compositions and were therefore probably of differing ages.

Interaction with the continental lithosphere. For the PST intrusions, the variations shown in Fig. 10 indicate that Sr- and Nd-isotopic variations were imposed on the magmas concomitant with fractional crystallization, by assimilation with fractional crystallization (AFC) or a similar process. The relationships shown in Fig. 10 require that Sr behaved incompatibly during fractional crystallization of the PST suite. The crystal cumulate formed during AFC cannot, therefore, have been plagioclase-rich. Least-squares modelling of the extract and evolved liquid from a starting composition with 9.6 weight % MgO (NGF16) to evolved composition with 6.78 weight % MgO (MHF5.1; Table 3) requires 21% crystallization of an assemblage of orthopyroxene (74.7%), plagioclase (18.9%) and minor augite (6.4%). With only 18.9% of the fractionating assemblage being plagioclase, DSr would have been <1 which is consistent with the relationship between 1/Sr and $^{87}Sr/^{86}Sr_{182}$ in Fig. 10. Consequently, to generate the range of Sr-isotopic compositions seen in the PST intrusions requires a source with $^{87}Sr/^{86}Sr_{182} \leq 0.7075$, and contaminants with $^{87}Sr/^{86}Sr_{182} > 0.7130$ and a range of εNd_{182}, which must be ≤ -6.0 for all samples.

Sr- and Nd-isotopic compositions for PST intrusions fall in an intermediate position between the data for CT1 basalts of Dronning Maud Land and the Karoo (Fig. 11). Luttinen & Furnes (2000) argued that the extreme Nd-isotopic compositions ($\varepsilon Nd_{182} \leq -17$) of CT1 basalts were the result of interaction between a mantle-derived magma and Archean (3.0 Ga) Grunehogna cratonic lithosphere (Fig. 1). Riley *et al.* (2006) used AFC and energy-constrained recharge AFC to model the isotopic compositions of Karoo basalts using an ORB-like source and an assimilant with $\varepsilon Nd_{182} = -4$ and $^{87}Sr/^{86}Sr_{182} = 0.710$, and showed that the observed isotopic variability in the basalts could be explained partly by these processes. In Fig. 11 three AFC trajectories are plotted and the parameters used to generate the curves are given in Table 4. These are not designed to fully explain the isotopic diversity in Gondwana low TiO_2 CFB, they have been generated in an attempt to constrain possible and impossible petrogenetic processes. The starting composition has been kept constant, and is based on that that of largely uncontaminated low TiO_2 basalts with $\varepsilon Nd_{182} = 2$ and $^{87}Sr/^{86}Sr_{182} = 0.7035$. For all three modelled AFC trends, the ratio of the country rock assimilated to crystal cumulate formed, *R*, has be set at 0.40, a value that is appropriate for crystallization in the middle- to upper-crust (Riley *et al.* 2006; Hole *et al*. 2015). D_{Sr} and D_{Nd} are set at 0.5 and 0.1 respectively, to simulate a cumulate with approximately 25% plagioclase, and 75% ferromagnesian minerals. This means that all three AFC trajectories approach the composition of the most contaminated magma for ≤ 20% AFC (Table 4). Increasing the value of *R* to 0.5 for any of the models does not significantly change the shape of the trajectories, but decreases the amount of AFC that is needed to reach the target compositions to ≤12%., and conversely, decreasing R to 0.3 requires ≤ 25% AFC. For the CT1 AFC model, the contaminant represents 3.0 Ga Grunehogen Craton (Fig. 1) felsic granulite, with $\varepsilon Nd_{182} = -50$ and $^{87}Sr/^{86}Sr_{182} = 0.712$ (felsic xenolith sample X4-AVL of Luttinen & Furnes 2000). The PST-1, mixing line intersects the lowest εNd_{182} samples in the PST suite, and the contaminant represents a 2.2 Ga Palaeoproterzoic felsic granulite with $\varepsilon Nd_{182} = -20$ and $^{87}Sr/^{86}Sr_{182} = 0.720$. The PST-2 mixing line, which also intersects the majority of data for Karoo basalts and lowest $^{87}Sr/^{86}Sr_{180}$ (~0.7090) Ferrar dolerites, representing mixing between a mantle-derived magma and 1.0-1.5 Ga felsic crust with εNd_{182} = -10. Plate reconstructions place the Falkland Islands mainly within the 1.0-1.5 Ga Namaqualand-Natal-Maudheim-Mozambique belt (Thistlewood *et al.* 1997) and on the continuation of the Cape Fold Belt (Fig. 1). Mesoproterozoic crust is therefore a likely candidate for basement to the Falkland Islands. What is also clear is that cratonic basement like that involved in the petrogensis of the CT1 basalts affects neither the PST intrusions nor Karoo low TiO_2 basalts. AFC models with geologically reasonable parameters and appropriate ages of potential basement contaminants can therefore produce the observed variations in the Sr- and Nd-isotopic characteristics of the PST intrusions for < 20% AFC.

Pyroxenite *versus* peridotite sources. PST intrusions with MgO > 8 weight % have lower CaO abundances (c. 8.5 weight %) than any other of the other Falkland Islands intrusions (Figs. 4 and 12). Such compositions are uncommon in continental flood basalts provinces. Orthopyroxene was the dominant fractionating phase during crystallization of the PST (Table 3) and estimates of more primitive compositions can be calculated by incrementally adding enstatite to a mafic PST composition. Addition of 30% enstatite to sample NGF16 yields magma with ~15 weight % MgO and ~7.5 weight % CaO. Compositions such as these are also found in the CT1 basalts of Dronning Maud Land (Figs 12 and 13). An unusual feature of the PST intrusions is their Si-oversaturated nature and high Cr content (Fig. 12) which is also reflected in unusually high Cr content of component orthopyroxene (e.g. enstatite in MHF3.2 has 0.74 weight % Cr_2O_3 at MgO/FeO = 2.8). In terms of major element compositions, PST intrusions bear strong similarities with magnesian andesite from continental subduction settings (e.g. Baker *et al.* 1994; Sato *et al.* 2014). For example, high-Mg andesites from Mt Shasta have a similar range of MgO to PST intrusions (Fig. 12) which is accompanied by SiO_2 = 51.5-54.0 weight %, Cr = 245-695 ppm, Ni =99-235 ppm, TiO_2 = 0.6-0.8 weight % and CaO =8.6-9.6 weight %. One mechanism that has been suggested for the production of high-Mg andesite is the interaction of slab-derived adakitic melts with mantle peridotite during subduction (Heinonen *et al.* 2014). A link to the previous subduction history of the mantle source from which Ferrar and Karoo basalts were derived has been made by a number of workers (e.g. Brewer *et al.* 1992; Storey *et al.* 1992; Heinonen *et al.* 2014) and in particular, the characteristic trough at Nb and Ta relative to adjacent elements (Fig. 9) has been interpreted as an inherited subduction signature.

Herzberg & Asimow (2008) note that primary magmas derived from the melting of pyroxenite will exhibit relative CaO depletion compared to melts from a peridotite source because of the dominance of residual clinopyroxene in the source region during partial melting of pyroxenite. Given the position that data for the PST occupy in Fig. 12, it seems clear that their major element compositions are not consistent with an origin by melting of mantle peridotite. It is well established that pyroxenite can be formed at the base of the lithosphere as a result of accumulation of mafic phases during basaltic magmatism (e.g. Downes *et al.* 2007). Such accumulative pyroxenite can yield magma by partial melting at some later stage, promoted by a new phase of mafic magmatism and by interaction with peridotite-derived melts (Lambart *et al.* 2013). The generation of silica-enriched pyroxenite melts is possible, which can yield Si-oversaturated melts like those of the PST intrusions (Lambart *et al.* 2013). It is therefore suggested that the PST were derived from a pyroxenite-rich source that was emplaced at the base of the lithosphere during the prolonged subduction history of Gondwana. Metasomatism of the pyroxenite by slab-derived fluids and melt, imparted a subduction signature to the pyroxenite. When subjected to the high mantle potential temperatures associated with the mantle plume beneath Dronning Maud Land at c. 180 Ma (T_P up to 1600°C; Heinonen *et al.* 2010), the pyroxenite underwent partial melting and produced the primary melt precursor to the PST intrusions. These melts then interacted with fusible, felsic continental crust to produce the geochemical composition of the more evolved PST compositions by AFC, or a related process. Extrapolation of the MgO - εNd_{180} trend for the PST to higher MgO contents (Fig. 10), suggests that a primitive composition with 15 weight % MgO might have had εNd_{180} ~0, and the correlation between 1/Sr and Sr-isotopic compositions requires the source to have $^{87}Sr/^{86}Sr_{182} \leq$ 0.7075.

DIT and Lively Island intrusions

In contrast to the PST intrusions, the sub-horizontal arrays delineated by DIT intrusions in Fig. 10a, suggests that AFC or a similar process was not important during their petrogenesis. However, a negative correlation between Th/Ta and εNd_{182} for the DIT intrusions (Fig. 10b) may require minor modification by a crustal component with Th/Ta ≥ 3.0. A characteristic feature of the DIT samples is that they have εNd_{182} in range -2.8 to +0.6, but with only a single analysed sample (NHF17) having $\varepsilon Nd_{182} < -1$. In addition, the Lively Island dyke, which falls close to the fractionation trend for the MFCT dolerites of the Transantarctic Mountains (Fig. 6), has Sr- and Nd-isotopic compositions ($^{87}Sr/^{86}Sr_{182}$ c. 0.7052, εNd_{182} = -0.5 to -1.4) that do not require the significant isotopic enrichment seen in the Ferrar dolerites (εNd_{182} in the range -3.3 to -5.3; Fleming *et al.* 1995). The source of the low TiO_2 DIT magmas could, therefore, have had $\varepsilon Nd_{182} > 0$, $^{87}Sr/^{86}Sr_{182} < 0.7050$, Th/Ta < 2.5 and La/Ta < 20. Nevertheless, there are striking similarities between the major trace element composition of the DIT and Lively Island intrusions and those of Ferrar dolerites of the Transantarctic and Theron mountains and the dolerites of Tasmania (e.g. Figs 6 and 13).

It has been argued that depleted mantle-like Os-isotopic signatures of Ferrar and Tasmanian dolerites, along with $\delta^{18}O$ of 5 to 7‰, are not consistent with an AFC process involving upper- or lower-crust, but are more likely to reflect source contamination involving interaction between mantle peridotite and recycled upper-crustal materials (Molzhan *et al.* 1996; Brauns *et al.* 2000). γ_{Os} values of -10 to +10 for harzburgite and lherzolite xenoliths from the sub-continental lithospheric mantle beneath SE Australia overlap with the range of γ_{Os} for the Tasmanian and Ferrar dolerites (γ_{Os} = -2 ± 25; these relatively large ranges in γ_{Os} reflect uncertainties in the estimates of initial $^{187}Os/^{188}Os$ ratios, rather than being a measured range of values). In addition, basalts and picrites from Dronning Maud Land have εNd_{182} = +8.0 to -2.2 and γ_{Os} in the range -1 to +10 reflecting a similar origin (Heinonen *et al.* 2010). It must be argued, therefore, that the unradiogenic Nd-isotopic compositions of the Ferrar dolerites must result from an ancient enrichment in Nd relative to Sm in their source, which may also have been accompanied by enrichment of the LILE relative to HFSE. It is therefore suggested that the DIT magmas were derived from a similar mantle source region to that of the Ferrar dolerites, but one which had experienced significantly less LILE and LREE enrichment to that that seen in the Transantarctic Mountains. Basalts from the Theron Mountains have εNd_{182} = -1.3 to -5.7, values which are transitional between those of the DIT intrusions and Ferrar dolerites (Brewer *et al.* 1992). There is, therefore, a geographical variability in LILE/HFSE and εNd_{182} is within the Jurassic low TiO_2 basalts of West Antarctica.

MAT intrusions

The positive εNd_{182} (2.7-3.6) and low Th/Ta, La/Ta and $[La/Yb]_N$ (0.8-1.0; 12.8-17.3 and 1.9-3.7 respectively) of MAT intrusions suggests that they were derived from an asthenospheric source, and escaped significant interaction with lithosphere. Such compositions are also known from the Southern Lebombo Rift and within Dronning Maud Land (Fig. 8). The most satisfactory explanation for the geochemical compositions of these rocks is that they were generated by decompression melting of the asthenosphere during the rifting stage of Gondwana break-up. In this respect they have similar geochemical compositions to the ORB-like Rooi Rand basaltic dykes of the southern Lebombo, which post-date the main magmatic phases in the region by about 5 Myr (Jourdan *et al.* 2007b).

Cretaceous intrusions

Until more data are forthcoming, the origin and affinity of the Cretaceous Teal Creek intrusion reported by Stone *et al.* (2009) remains somewhat obscure. Major element data for the intrusion plot close to the Theron Mountains low TiO_2 trend in Fig. 5, but the intrusion has higher Fe_2O_3 (c. 15.9 weight %) at 5.7 weight % MgO than any of the data for the intrusions presented here. What is clear, is that there is an extensive suite of low TiO_2 basalts within the Etendeka Province (e.g. Gibson *et al.* 2005; Thompson *et al.* 2001) from which it could be sourced. However, none of the groups of intrusions described here carries a similar signature to that presented by Stone *et al.* (2009) for the Teal Creek dyke.

Mantle potential temperature, rifting and magmatism

Fig. 14a summarizes the available data for olivine equilibration temperatures (T_{OL}) for MAT and E-W basalts and picrites from Dronning Maud. MAT and E-W basalts yield olivine equilibration temperatures of 1245°C and 1330°C respectively, using the method of Putirka *et al.* (2007), whilst olivine in picrites from Dronning Maud Land yield T_{OL} up to 1450°C. Converting equilibration temperatures to T_P is problematical if the pressure and extent of melting cannot be independently determined (Herzburg & Asomow 2008; Herzburg & Gazel 2009; Hole 2015), which they cannot for the MAT and E-W samples. However, since olivine equilibration temperature increases with increasing pressure of crystallization, synthetic olivine liquidi can be calculated for any given temperature and pressure (Herzberg & Gazel 2009). Fig. 13b shows the inferred temperature-pressure conditions at which fractional melting terminated for calculated primary magmas from Dronning Maud Land, the Karoo Province of southern Africa, Ferrar dolerites of Antarctica calculated following the methods of Herzberg & Gazel (2009) and Hole (2015).

Also shown in Fig. 13 for are data for basalts from the Cretaceous Etendeka Province of SW Africa (Kieding *et al.* 2011) for which estimates of T_{OL}, estimates of T_P from melt inclusions in ultra-magnesian olivine, and estimates of T_P from the PRIMEL2 model of Herzberg & Asimow (2008) have all been calculated on the same samples. Using the Herzberg & Asimow (2008) model yields T_P = 1500-1550°C and final pressures of melting (P*f*) between 1.5 and 4.0 GPa (Fig. 13a). T_P from melt inclusions is 1300-1520°C, whilst T_{OL} is in the range 1250-1400°C and there is an empirical relationship between T_{OL} and melt inclusion T_P which approximates to $T_P = 1.443\ T_{ol} - 501$ for the Etendeka plume system (Fig. 13c). Therefore is seems that within a single plume system, basalts may be generated over ranges of T_P that are larger than the ±50°C error inherent in the calculation methods (Herzberg & Asimow 2009; Hole 2015). Direct application of this empirical observation to the Dronning Maud Land picrites suggest maximum $T_P \sim 1550$°C, a temperature that is considered to be associated with 'hot' mantle plumes such as Iceland at 60 Ma (Fig. 13a; Herzberg & Gazel 2009). However, indications of T_P ~1300°C are also evident from the Dronning Maud Land data. For Falkland Islands E-W basalts, T_{OL} ~ 1330°C, which implies T_P ~1400°C and for olivine-phyric MAT basalts, T_{OL} ~1250°C implying T_P ~1300°C. These T_P estimates for the Falkland Islands E-W and MAT basalts may therefore be reconciled with a model involving melting of mantle with near-ambient temperature ($T_P \geq$ 1350°C), but would require intersection of the dry peridotite solidus at ~2.1 GPa (~70km) and all melting to take place in the garnet stability field of the mantle; the most mafic MAT and E-W intrusions have $[La/Yb]_N$ <2.0 which does not preclude such an origin. Additionally, near-ambient T_P melting would require the continental lithosphere to be thinned substantially and perhaps to < 50km, to allow decompression melting to take place. Gondwana fragmentation could have provided the necessary extensional tectonism to allow for such lithospheric thinning. Whilst there is no primary evidence to suggest T_P was > 1450°C beneath the Falkland Islands at 180 Ma, it is possible that high-MgO large melt fractions requiring substantially higher T_P exist in the region, but they have not been sampled, remains a possibility.

The diversity of magma types found in the Falkland Islands, and the position of the islands in a 180 Ma plate reconstruction (Fig. 1) is entirely consistent with the their being close to the focus of magmatism during continental break-up. We concur with Brewer *et al*. (1992) and Riley *et al*. (2006) that there is considerable overlap in the geographical distribution of the Ferrar and Karoo LIPs, which is most obvious in the Theron Mountains. It is also clear, that despite the wealth of geochemical data available for the Transantarctic Mountains and

Tasmania, there is no evidence to suggest that volcanic rocks with affinities to the Karoo LIP occur in those areas. The broadly linear distribution of Ferrar LIP volcanic rocks has been attributed to syn- or pre-volcanic rifting (Elliot 2013) with lava flows fed from shallow (< 4 km depth) sills intruding Early Jurassic Mawson Group and equivalent sedimentary rocks (Muirhead *et al.* 2014). Pillow basalts and palagonite successions, at the base of the lava pile along with the substantial thickness of many lava flows in the Transantarctic Mountains, suggest confining topography and emplacement into a rift system (Elliot 2013). Stratigraphical confinement of early magmatism to extensional basins is a feature of a number of LIPs (e.g. North Atlantic Igneous Province, Williamson & Bell 2012; Hole *et al.* 2015; Central Atlantic Magmatic Province; Coltice *et al.* 2009; Hole 2015). Emplacement of Ferrar magmas into an active rift is therefore consistent with the magmatic plumbing (Muirhead *et al.* 2014), the style of volcanic activity at the base of the system, and the linear distribution of volcanism. In addition, Storey *et al.* (1988) also noted that Ferrar basaltic volcanism was synchronous with within-plate granitic magmatism in the Ellsworth Mountains (Fig. 1), sodic-alkaline intrusions being emplaced through dilated crust in rift-controlled loci. It has also been argued that some of the most magnesian Ferrar dolerites were generated by decompression melting of internally heated mantle in an active rift zone beneath which mantle potential temperature (T_P) was 1450 ± 50°C (Hole 2015). If this is the case, then the action of a hot mantle plume is not required for Ferrar magmatism (Hole 2015) and may also not be required for magmatism in the Falkland Islands which were situated on an extension of the Ferrar-Theron Mountains rift system at 180 Ma.

With the exception of the ORB-like basalts of the Rooi Rand dyke swarm (Marsh *et al.* 1997; Mitchell *et al.* 1999) which represent syn-break-up magmas, Karoo magmatism does not appear to be geographically restricted in the same manner as Ferrar magmatism, and basalts with Karoo-type geochemical compositions only extend as far as the overlap zone in the Theron Mountains. In addition, along the zone of the Ferrar LIP, continental break-up failed, whereas the Karoo was close to the locus of the formation of three triple junctions (Fig. 1). It is therefore suggested that Ferrar LIP magmatism was limited to the zone of extensional tectonism, extension being driven by plate-boundary forces in a similar manner to that which controls part of the NAIP (Nielsen *et al.* 2007; Hole *et al.* 2015). Within this rift, magmatism occurred because of decompression melting of internally heated mantle. Conversely, the high mantle potential temperatures (T_P up to 1550°C) required for the generation of some Dronning Maud Land break-up related picrite magmas (Heinonen & Luttinen 2010) suggests proximity to a plume head. It was this plume head that drove the break-up Antarctica and South Africa, but the Falkland Islands would have been on its periphery, as would the Theron Mountains.

Conclusions

The Jurassic (c. 182 Ma) intrusions of the Falkland Islands exhibit a broad range of geochemical compositions that encompass much of the variability seen in the Karoo and Ferrar LIPs. PST intrusions were derived from by melting of a pyroxenite-rich source that had been enriched in LILE during the prior subduction history of this part of Gondwana. Magmas subsequently interacted with 'old' (c. 2.2 Ga) fusible continental lithospheric components by a AFC or a related process. DIT intrusions have trace element signatures that are very similar to volcanic rocks of the Ferrar LIP, but some samples have noticeably unradiogenic Sr- and radiogenic Nd-isotopic compositions ($^{87}Sr/^{86}Sr_{182}$ ~ 0.7050 and εNd_{182} ~0) compared to most other Ferrar LIP igneous rocks. This suggests that the source of the Ferrar dolerites is not necessarily particularly isotopically enriched. Basalts with radiogenic Nd- and unradiogenic Sr-isotopic compositions ($^{87}Sr/^{86}Sr_{182}$ <0.7045 and εNd_{182} +4) also have Th/Ta and La/Ta (~1.0 and 17 respectively) that require little input from the continental lithosphere. These basalts were probably emplaced syn-break-up and are likened to the Rooi Rand dykes of the Southern Lebombo of Africa.

Early Jurassic plate reconstructions place the Falkland Islands close to the Weddell Triple Junction, at the proximity of the islands to the area of overlap between Karoo and Ferrar LIPs explains the diversity of igneous rock compositions. Whilst Ferrar and Karoo LIP igneous rocks show overlapping distributions in the Theron Mountains Falkland Islands and southern Africa, there is no evidence for Karoo-type magmas within the majority of the Ferrar LIP. In addition, whilst there are basalts within the Karoo LIP that require T_P ≥1550°C, the Ferrar LIP, and equivalent magma types in the Falkland Islands (i.e. DIT intrusions) were unrelated to a mantle plume and were formed by decompression melting of internally heated mantle with T_P ≤1450°C. The Ferrar LIP was emplaced into actively extending continental lithosphere, with extension being driven by pre-break-up plate boundary forces. The Karoo province owes its existence to a hot mantle plume that was centred near the boundary of what is now Dronning Maud Land and the eastern part of South Africa. The diversity of the magmatism in the Falkland Islands has its origins in the fact that the islands occupied a position towards the extremity of both the rift system and the extremity of the plume system centred on Dronning Maud Land.

References Cited.

Antonini, P., Piccirillo, E.M., Petrini, R., Civetta, M., D'Antonio, M. & Orsi, G. 1999. Enriched mantle Dupal signature in the genesis of the Jurassic Ferrar tholeiites from the Prince Albert Mountains, (Victoria Land, Antarctica). *Contributions to Mineralogy and Petrology*, **136**, 1-19.

Baker, M.B., Grove, T.L. and Price, R.C. 1994. Primitive basalts and andesites from the Mt. Shasta region, N. California: products of varying melt fraction and water content. *Contributions to Mineralogy and Petrology*, **118**, 111-129.

Baranov, A. & Morelli. A. 2013. The Moho depth map of Antarctica. *Tectonophysics*, **609**, 299-313.

Brauns, C.M., Hergt, J.M. Woodhead, J.D. & Maas, R. 2000. Os isotopes and the origin of the Tasmanian dolerites. *Journal of Petrology*, **41**, 905-918.

Brewer, T. S., Hergt, J. M., Hawkesworth, C. J., Rex D. C. & Storey B. C. 1992. Coats Land dolerites and the generation of Antarctic continental flood basalts. *In:* Storey, B. C., Alabaster, T. & Pankhurst, R. J. (eds) *Magmatism and the causes of Continental Break-Up* Geological Society, London, Special Publications, **64,** 185-208.

Coltice, N., Bertrand, H., Rey, P.M., Jourdan, F., Phillips, B.R. & Ricard, Y. 2009. Global warming of the mantle beneath continents back to the Archaean. *Gondwana Research*, **15**, 254-266.

Demarchi, G., Antonini, P., Piccirillo, E.M., Orsi, G., Civetta, L. & D'Antonini, M. 2001. Significance of orthopyroxene and major element constraints on the petrogenesis of Ferrar tholeiites from southern Prince Albert Mountains, Victoria Land, Antarctica. *Contributions to Mineralogy and Petrology*, **142**, 127-146.

Downes, H., Upton, B.G.J., Connolly, J., Beard, A.D. & Bodinier, J-L 2007. Evidence for late Palaeozoic crustal underplating beneath SW Scotland Petrology and geochemistry of a cumulate xenolith suite from Bute. *Journal of the Geological Society, London*, **164**, 1217-1231.

Elliot, D.H. 2013. The geological and tectonic evolution of the Transantarctic Mountains: a review. *In:* Hambrey, M.J., Barker, P.F., Barrett, P.J., Bowman, V., Davies, B., Smellie, J.L. & Tranter, M (eds). *Antarctic Palaeoenvironments and Earth-surface process*. Geological Society London, Special Publications, **381**, 7-35.

Elliot, D. H. & Fleming, T. H. 2000. Weddell Triple Junction: The principal focus of Ferrar and Karoo magmatism during the initial break-up of Gondwana. *Geology*, **28**, 539-542.

Elliot, D. H. & Fleming, T. H. 2004. Occurrence and Dispersal of Magmas in the Jurassic Ferrar Large Igneous Province, Antarctica. *Gondwana Research*, B, 223-237.

Elliot, D.H., Fleming, T.H., Haban, M.A. & Siders, M.A. 1995. Petrology and mineralogy of the Kirkpatrick Basalt and Ferrar Dolerite, Mesa Region, Northern Vitoria Land, Antarctica. *In*: Elliot, D.H. & Blaisdell, L.L. (eds) *Contribution to Antarctic Research IV*. Antarctic Research Series, 67. American Geophysical Union, Washington DC, 103-141.

Elliot, D. H., Fleming, T. H., Kyle, P. R. & Foland, K. A. 1999. Long-distance transport of magmas in the Jurassic Ferrar large igneous province, Antarctica. *Earth and Planetary Science Letters*, **167**, 89–104.

Encarnacion, J., Fleming, T.H., Elliot, D.H. & Eales, H. 1996. Synchronous emplacement of Ferrar and Karoo dolerites and the early breakup of Gondwana. *Geology*, **24**, 535-539.

Fleming, T.H., Foland, K.A. & Elliot, D.H. 1995. Isotopic and chemical constraints on the crustal evolution and source signature of Ferrar magmas, north Victoria Land, Antarctica. *Contributions to Mineralogy and Petrology*, **121**, 217-236.

Fleming, T.H., Heinmann, A., Foland K.A. & Elliot, D.H. 1997. $^{40}Ar/^{39}Ar$ geochronology of Ferrar Dolerite sills from the Transantarctic Mountains, Antarctica: Implications for the age and origin of the Ferrar magmatic province. *Bulletin of the Geological Society of America*, **109**, 533-546.

Galerne,C.Y., Nuemann, E-R. & Planke, S. 2008. Emplacement mechanisms of sill complexes: Information from the geochemical architecture of the Golden Valley Sill Complex, South Africa. *Journal of Volcanology and Geothermal Research*, **177**, 425-440.

Gibson, S.A., Thompson, R.N., Day, J.A., Humphris, S.E. & Dickin A.P. 2005. Melt-generation associated with the Tristan mantle plume: constraints on the origin of EM-1. *Earth and Planetary Science Letters*, **237**, 744-767.

Greenway, M. E., 1972. The geology of the Falkland Islands. *British Antarctic Survey Scientific Reports*, **76**, 42 pp.

Harris, C., Marsh, J.S., Duncan, A.R. & Erlank, A.J. 1990. The Petrogenesis of the Kirwan Basalts of Dronning Maud Land, Antarctica. *Journal of Petrology*, **31**, 341-369.

Heinonen, J.S. & Luttinen, A.V. 2008. Jurassic dikes of Vestfjella, western Dronning Maud Land, Antarctica: Geochemical tracing of ferropicrite sources. *Lithos*, **105**, 347-364.

Heinonen, J.S., Carlson, R.W. & Luttinen, A.V. 2010. Isotopic (Sr, Nd, Pb, and Os) composition of highly magnesian dikes of Vestfjella, western Dronning Maud Land, Antarctica: A key to the origins of the Jurassic Karoo large igneous province? *Chemical Geology*, **277**, 227-244.

Heinonen, J.S., Luttinen, A.V., Riley, T.R. & Nichallik, R.M. 2013. Mixed pyroxenite–peridotite sources for mafic and ultramafic dikes from the Antarctic segment of the Karoo continental flood basalt province. *Lithos*, **177**, 266-380.

Heinonen, J.S., Carlson, R.W., Riley, T.R., Luttinen, A.V. & Horan, M.F. 2014. Subduction-modified oceanic crust mixed with a depleted mantle reservoir in the sources of the Karoo continental flood basalt province. *Earth and Planetary Science Letters*, **394**, 229-241.

Hergt J. M., Chappell B. W., Mcculloch M. T., McDougall I. & Chivas A. R. 1989. The geochemistry of Jurassic dolerites from Portal Peak, Antarctica. *Contributions to Mineralogy and Petrology*, **102**, 298-305.

Herzberg, C. & Asimow, P.D. 2008. Petrology of some oceanic island basalts: PRIMELT2.XLS software for primary magma calculation. *Geochemistry, Geophysics, Geosystems*, **9**.

Herzberg, C. & Gazel, E. 2009. Petrological evidence for secular cooling in mantle plumes. *Nature*, **458**, 619-623.

Hole, M.J. 2015. The generation of continental flood basalts by decompression melting of internally heated mantle. *Geology*, **43**.

Hole, M.J., Millett, J.M., Rogers, N.W. & Jolley, D.W. 2015. Rifting and mafic magmatism in the Hebridean basins. *Journal of the Geological Society, London,* **172**, 218-236.

Jourdan, F., Féraud, F.G., Bertrand, H., Kampunzu, A.B., Tshoso, Le Gall, G.B., Tiercelin, J.J. & Capiez P, 2004. The Karoo triple junction questioned: evidence from Jurassic and Proterozoic $^{40}Ar/^{39}Ar$ ages and geochemistry of the giant Okavango dyke swarm (Botswana). *Earth and Planetary Science Letters*, **222**, 989-1006.

Jourdan, F., Féraud, G., Bertrand, H., Kampunzu, A.B., Tshoso, G., Watkeys, M.K. & Le Gall, B. 2005. Karoo large igneous province: Brevity, origin and relation to mass extinction questioned by new $^{40}Ar/^{39}Ar$ age data. *Geology*, **33**, 745–748.

Jourdan, F., Féraud, G., Bertrand, H., Watkeys, M.K. & Renne, P.R. 2007a. Distinct brief major events in the Karoo large igneous province clarified by new $^{40}Ar/^{39}Ar$ ages on the Lesotho basalts. *Lithos*, **98**, 195-209.

Jourdan F., Bertrand H., Schärer U., Blichert-Toft J., Feraud G. & Kampunzu A.B. 2007b. Major and trace element and Sr, Nd, Hf, and Pb isotope compositions of the Karoo large igneous province, Botswana-Zimbabwe: lithosphere *vs* mantle plume contribution. *Journal of Petrology*, **48**, 1043-1077

Keiding, J.K., Trumbull, R.B., Veksler, I.V. & Jerram, D.A. 2011. On the significance of ultra-magnesian olivines in basaltic rocks. *Geology*, **39**, 1095-1098.

Lambart, S., Lapporte, D. & Schiano, P. 2013. Markers of the pyroxenite contribution in the major-element compositions of oceanic basalts: Review of the experimental constraints. *Lithos*, **160-161**, 14-36.

Luttinen, A.V. & Furnes, H., 2000. Flood basalts of the Vestfjella: Jurassic magmatism across an Arcehan-Proterozoic lithospheric boundary in Dronning Maud Land, Antarctica. *Journal of Petrology*, **41**, 1271-1305.

Luttinen, A.V., Ramo, O.T. & Huhma, H. 1998. Neodymium and strontium isotope and trace element composition of a Mesozoic CFB suite from Dronning Maud Land, Antarctica: implications for lithosphere and asthenosphere contributions to Karroo magmatism. *Geochimica et Cosmochimica Acta,* **15**, 2701-2714.

Macdonald, D.I.M., Gomez-Perez, I., Frnazese, J., Spalleti, L., Lawver, L., Gahagan, L., Dalziel, I.W.D., Thomas, C.J., Trewin, N.H., Hole, M.J. & Paton, D. 2003. Mesozoic break-up of SW Gondwana: implications for regional hydrocarbon potential of the southern South Atlantic. *Marine & Petroleum Geology*, **20**, 287-308

Marsh, J.S., Hooper, P.R., Rehacek, J., Duncan, R.A. & Duncan, A.R. 1997. Stratigraphy and age of Karroo basalts of Lesotho and implications for correlations within the Karroo Igneous Province. In: Mahoney, J.J. & Coffin, M.F. (eds*) Large Igneous Provinces*, A G U Geophysical Monographs, 100, 247-272.

McClintock, M., Marsh, J. & White, J.D.L. 2008. Compositionally diverse magmas erupted close together in space and time within a Karoo flood basalt crater complex. *Bulletin of Volcanology*, **70**, 923-946.

Melluso L., Cucciniello C., Petrone C.M., Lustrino M., Morra V., Tiepolo M. &Vasconcelos L. 2008. Petrology of Karoo volcanic rocks in the southern Lebombo monocline, Mozambique. *Journal of African Earth Sciences*, **52**, 139-151.

Melluso, L., Hergt, M.J. & Zanetti, A. 2013. The late crystallization stages of low-Ti, low-Fe tholeiitic magmas:Insights from evolved Antarctic and Tasmanian rocks. *Lithos*, **188**, 72-83.

Mitchell, C., Ellam, R.M. & Cox, K.G. 1999. Mesozoic dolerite dykes of the Falkland Islands: petrology, petrogenesis and implications for geochemical provinciality in Gondwanaland low-Ti basaltic rocks. *Journal of the Geological Society, London*, **156**, 901-916.

Molzahn, M., Reisberg, L. & Wörner, G. 1996. Os, Sr, Nd, Pb, O isotope and trace element data from the Ferrar flood basalts, Antarctica: evidence for an enriched subcontinental lithospheric source. *Earth and Planetary Science Letters*, **144**, 529-546.

Muirhead, J.D., Airoldi, G., White, J.L. and Rowland, J.V. 2014. Cracking the lid: Sill-fed dikes are the likely feeders of flood basalt eruptions. *Earth and Planetary Science Letters*, **406**, 187-197.

Mussett, A.E. & Taylor, G.K. 1994. ^{40}Ar-^{39}Ar ages for dykes from the Falkland Islands with implications for the break-up of southern Gondwanaland. *Journal of the Geological Society, London,* **151**, 79-81.

Nielsen, S.B., Stephenson, R.A. & Thomsen, E. 2007. Dynamics of Mid-Palaeocene North Atlantic rifting linked with European intra-plate deformations. *Nature*, **450**, 1071-1074

Nuemann, E-R., Svensen, H., Galerne, G.Y. & Planke, S. 2011. Multistage Evolution of Dolerites in the Karoo Large Igneous Province, Central South Africa. *Journal of Petrology*, **52**, 959-984.

Putirka, K.D., Perfit, M., Ryerson, F.J. & Jackson, M.G. 2007. Ambient and excess mantle temperatures, olivine thermometry, and active vs. passive upwelling. *Chemical Geology*, **241**, 177-206.

Richards, P.C., Stone, P., Kimbell, G.S., Mcintosh, W.C. & Phillips, E.R. 2013. Mesozoic magmatism in the Falkland Islands (South Atlantic) and their offshore sedimentary basins. *Journal of Petroleum Geology*, **36**, 61-74.

Riley, T.R., Curtis, M.L., Leat, P.T., Watkeys, M.K., Duncan, R.A., Millar, I.L. & Owens, W.H. 2006. Overlap of Karoo and Ferrar Magma Types in KwaZulu-Natal, South Africa. *Journal of Petrology*, **47**, 541-566.

Riley, T.R., Millar, I.L., Watkeys, M.K., Curtis, M.L., Leat, P.T., Klausen, M.B. & Fanning, C.M. 2004. U-Pb zircon (SHRIMP) ages for the Lemombo rhyolites, South Africa: refining the duration of Karoo magmatism. *Journal of the Geological Society, London,* **161**, 547-550.

Sushchevskaya, N.M., Korago, E.A., Belyatsky, B.V. & Sirotkin, A.N. 2009. Evolution of the Karoo-Maud mantle plume in Antarctica and its influence on the magmatism of the early stages of Indian ocean opening. *Geochemistry International*, **47**, 1-17.

Stone, P., Kimbell, G.S. & Richards, P.C. 2009. Rotation of the Falklands microplate reassessed after recognition of discrete Jurassic and Cretaceous dyke swarms. *Petroleum Geoscience*, **15**, 279-287.

Stone, P., Richards, P.C., Kimbell, G.S., Esser, R.P.,& Reeves, D. 2008 Cretaceous dykes discovered in the Falkland Islands: implications for regional tectonics in the South Atlantic. *Journal of the Geological Society, London,* **165**, 1-4

Storey, B.C., Hole, M.J., Pankhurst, R.J., Millar, I.L. & Vennum, W. 1988. Middle Jurassic within-plate granites in West Anratctica and their bearing on the break-up of Gondwana. *Journal of the Geological Society, London*, **145**, 999-1007.

Storey, B.C., Alabaster, T., Hole, M.J., Pankhurst, R.J. & Wever, H. 1992. Role of subduction-plate boundary forces during the initial stages of Gondwana break-up: Evidence from the proto-Pacific margin of Antarctica. *In:* Storey, B. C., Alabaster, T. & Pankhurst, R. J. (eds) *Magmatism and the causes of Continental Break-Up* Geological Society, London, Special Publications, **64,** 149-163.

Sweeney R. J., Duncan A. R., Erlank A. J. 1994. Geochemistry and Petrogenesis of Central Lebombo basalts of the Karoo igneous province. *Journal of Petrology*, **35** 95-125.

Sun, S-S. & Mcdonough, W. F. 1989. Chemical and isotopic systematics of oceanic basalts: implications for mantle composition and processes. In: Saunders, A.D. & Norry, M.J., (eds). *Magmatism in the ocean basins*. Geological Society, London, Special Publications, **42,** 313-345.

Sushchevskaya, N. M., Belyatskii, B. V., Leichenov, G. L. & Laiba A. A. 2009. Evolution of the Karoo-Maud plume in Antarctica and its influence on the magmatism of the early stages of Indian Ocean opening. *Geochemistry International*, **47**, 1-17

Thistlewood, L., Leat, P. T., Millar, I.L., Storey, B.C. & Vaughan, A. P. M. 1997. Basement Geology and Palaeozic-Mesozoic mafic dykes from the Cape Meredith Complex, Falkland Islands: a record of repeated intracontinental extension. *Geological Magazine,* **134**, 355-367.

Thompson, R.N., Gibson, S.A., Dickin, A.P. & Smith, P.M. 2001. Early Cretaceous basalt and picrate dykes of the Southern Etendeka region, NW Namibia: windows into the role of the Tristan plume in Parana-Etendeka magmatism. *Journal of Petrology*, **42**, 2049-2081.

Wilhelm, S. & Wörner, G. 1996. Crystal size distribution in Jurassic Ferrar flows and sills (Victoria Land, Antarctica): evidence for processes of cooling, nucleation and crystallization. *Contributions to Mineralogy and Petrology*, **125**, 1-15.

Williamson, I.T. & Bell, B.R. 2012. The Staffa Lava Formation: graben-related volcanism, associated sedimentation and landscape character during the early development of the Palaeogene Mull Lava Field, NW Scotland. *Scottish Journal of Geology*, **48**, 1-46.

Figure Captions

Figure 1. a) Reconstruction of Southern Gondwana immediately prior to break-up at c. 180 Ma. MEB, Maurice Ewing Bank; EWM, Ellsworth-Whitmore Mountains; AP, Antarctic Peninsula; SA, South Africa; SAM, South America; ANT, Antarctica. Position of the Weddell, Limpopo and Lower Zambesi triple junctions are from Elliot & Fleming (2000). Ar-Ar ages, this study and Stone *et al.* (2009). After Macdonald *et al.* (2003). b) Map showing the distribution of break-up related igneous rocks of Antarctica. Fine pecked lines are contours for depth to the Moho (Baranov & Morelli 2013), and the grey pecked lines encompass the region of the Ferrar Igneous Province according to Elliot (2013).

Figure 2. Map of the Falkland Islands showing the distribution of magnetic anomalies and main trends of dyke swarms. Solid or pecked lines do not necessarily represent continuous exposure of dykes. Inset; azimuths of Dykes in the South Harbour area of West Falkland. The rectangle at South Harbour is the area covered by the map in the supplementary material, which gives the sample locations in that area. After Stone *et al.* (2009) and Richards *et al.* (2013). Ar-Ar ages (this study, Stone *et al.* 2008; 2009) and sample locations in East Falkland which are mentioned in the text, are indicated.

Figure 3. Ar-Ar step-heating spectrum for plagioclase in sample WI-5.

Figure 4. a) Major (weight %) and trace element (in ppm) variations *versus* MgO weight % in Falkland Islands dykes. Filled dots, Port Sussex Creek type (PST) NE-SW two-pyroxene dolerites; open triangles, E-W olivine dolerite dykes; open squares, Lively Island dyke; filled squares, Mount Alice-type (MAT) dykes; open dots, low TiO_2 DIT intrusions; filled diamonds, high TiO_2 DIT intrusions; open diamonds, evolved sheets from the South Harbour-Dyke Island transect (Dyke Island Type; DIT); crosses, Pony's Pass N-S Cretaceous dyke (Stone *et al.* 2008). Data from this study, Mitchell *et al.* (1999) and Thistlewood *et al.* (1997).

Figure 5. a) Pyroxene end-member compositions represented in the quadrilateral system Enstatite - Ferrosilite – Wollastonite for Falkland Islands intrusions (this study and Mitchell *et al.* 1999) and dolerites from the Transantarctic Mountains (Elliot 1995; Demarchi *et al.* 2001). MFCT, Mount Fazio Chemical Type; SPCT, Scarab Peak Chemical Type; NVL, Northern Victoria Land.

Figure 6. Ti/Zr *versus* SiO_2 and TiO_2 *versus* MgO, for Falkland Islands dykes (symbols as for Fig. 4), Ferrar LIP dolerites and Dronning Maud land volcanic rocks. Data sources; Transantarctic Mountains and Theron Mountains; Hergt *et al.* (1989), Brewer *et al.* (1992), Elliot *et al.* (1995), Fleming *et al.* (1995), Molzahn *et al.* (1996), Wörner *et al.* (1996), Antonini

et al. (1999), Elliot *et al.* (1999), Elliot & Fleming (2004), Wilhelm & Worner (1996). Dronning Maud Land; Heinonen & Luttinen (2008); Luttinen *et al.* (1998), Luttinen & Furnes (2000), Heinonen *et al.* (2010; 2013; 2014). Kirwanveggan; Harris *et al.* (1990).

Figure 7. a) Chondrite-normalized REE profiles for representative samples of a) PST, MAT and E-W intrusions; b) DIT intrusions.

Figure 8. a) to d) Multi-element ORB-normalized (Sun & McDonough 1989) variation diagrams for Falkland Islands dykes. Comparable basalts from other regions of the low TiO_2 Gondwana LIP are shown by grey lines. Sample SA.6.1 (South Africa), Riley *et al.* (2006); VF111-85, CT3 basalt, Dronning Maud Land (Luttinen & Furnes 2000); 47206-3, low TiO_2 tholeiite from Schirmacher Oasis, Dronning Maud Land (Sushchevskaya *et al.* 2009); Average SPCT from Elliot *et al.* (1995).

Figure 9. a) εNd_{182} *versus* $^{87}Sr/^{86}Sr_{182}$; b) $^{207}Pb/^{204}Pb$ *versus* $^{206}Pb/^{204}Pb$ for Falkland Islands dykes. c) εNd_{182} *versus* $^{207}Pb/^{204}Pb$ for Falkland Islands intrusions. Symbols as for Fig. 4. Data sources this study, Mitchell *et al.* (1999) and Thistlewood *et al.* (1997).

Figure. 10 a) and b) εNd_{182} and $^{87}Sr/^{86}Sr_{182}$ *versus* MgO; c) εNd_{182} versus Th/Ta and d) $^{87}Sr/^{86}Sr_{182}$ *versus* 1/Sr for Falkland Islands intrusions. Symbols as for Fig. 4 except grey dots are for the lowest reported Th/Ta for Ferrar dolerites (Fleming *et al.* 1995). Parameters for the AFC mixing line are given in Table 4 with % AFC given on the mixing line.

Fig. 11. a) εNd_{182} *versus* $^{87}Sr/^{86}Sr_{182}$ for Falkland Islands PST intrusions (filled dots) Karoo low TiO_2 volcanic rocks (open circles), Dronning Maud Land CT1 (open triangles), CT2 (filled diamonds) and CT3 (filled triangles) basalts. Details of the parameters used in generating the three AFC mixing lines (CT1, PST-1 and PST-2) are given in Table 4. Each cross represents 1% AFC. Data sources for Karoo Province; Galerne *et al.* (2008); McClintock *et al.* (2008); Neumann *et al.* (2011).

Figure 12. a) CaO *versus* MgO (weight %) for Falkland Islands intrusions (black dots PST; grey dots, DIT; grey squares MAT; grey triangles, E-W) and Dronnning Maud Land high MgO, silica-oversaturated CT1 basalts (circles). The dividing line between melts derived from peridotite and pyroxenite sources is taken from Herzberg & Asimow (2008). Lines with crosses and arrows represent the effect of accumulation of the phase indicated on the composition of PST basalt NEF9, with each cross representing 5% accumulation. b) Cr (ppm) *versus* SiO_2 for Falkland Islands intrusions (symbols as for Fig. 4) and high-Mg andesites from Mt Shasta (crosses; Baker *et al.* 1994).

Figure 13. a) Olivine equilibration temperatures (°C) *versus* Mg# of liquid in equilibrium with olivine for Ahlmannryggen dykes (filled dots; Heinonen & Luttinen 2008), Vestfjella high TiO_2 ferropicrite (filled triangles; Heinonen *et al.* 2013), Etendeka picrite (open squares; Kieding *et al.* 2011) and Falklands Islands MAT (star in circle) and E-W (open triangles) intrusions. Olivine equilibration temperatures have been calculated according to the scheme of Putirka *et al*. (2007). Vertical lines connecting points for Ahlmannryggen samples are calculated equilibration temperatures for different olivine phenocrysts in individual whole-rock samples. Figures in italics are T_P from melt inclusions for Etendeka samples plotted in Fig. 13b (Kieding *et al.* 2011). b) T_P calculated from melt inclusions in ultra-magnesian olivines from the Etendeka Provice *versus* olivine equilibration temperatures for the same samples. Data from Keiding *et al.* (2011). c) Inferred temperature-pressure conditions at which fractional melting terminated for calculated primary magmas from Dronning Maud Land, the Karoo Province of southern Africa, Ferrar dolerites of Antarcitca and picrites of the Etendeka Province of western Africa. The diagram was constructed following the methods of Herzberg and Gazel (2009) and Hole (2015). Samples with MgO > 20 weight % are shown schematically following an adiabatic pathway for T_P = 1640°C. The diagonally shaded box on the temperature axis is the range of olivine equilibration temperatures, calculated at 0 GPa, for olivine in ferro-picrite dykes from Dronning Maud following the method of Putirka et al. (2007), and the box labelled 'MAT & E-W' is the same calculations for MAT and E-W intrusions. Adiabatic melting paths are labelled with mantle potential temperature. 2σ error bars are from Hole (2015).

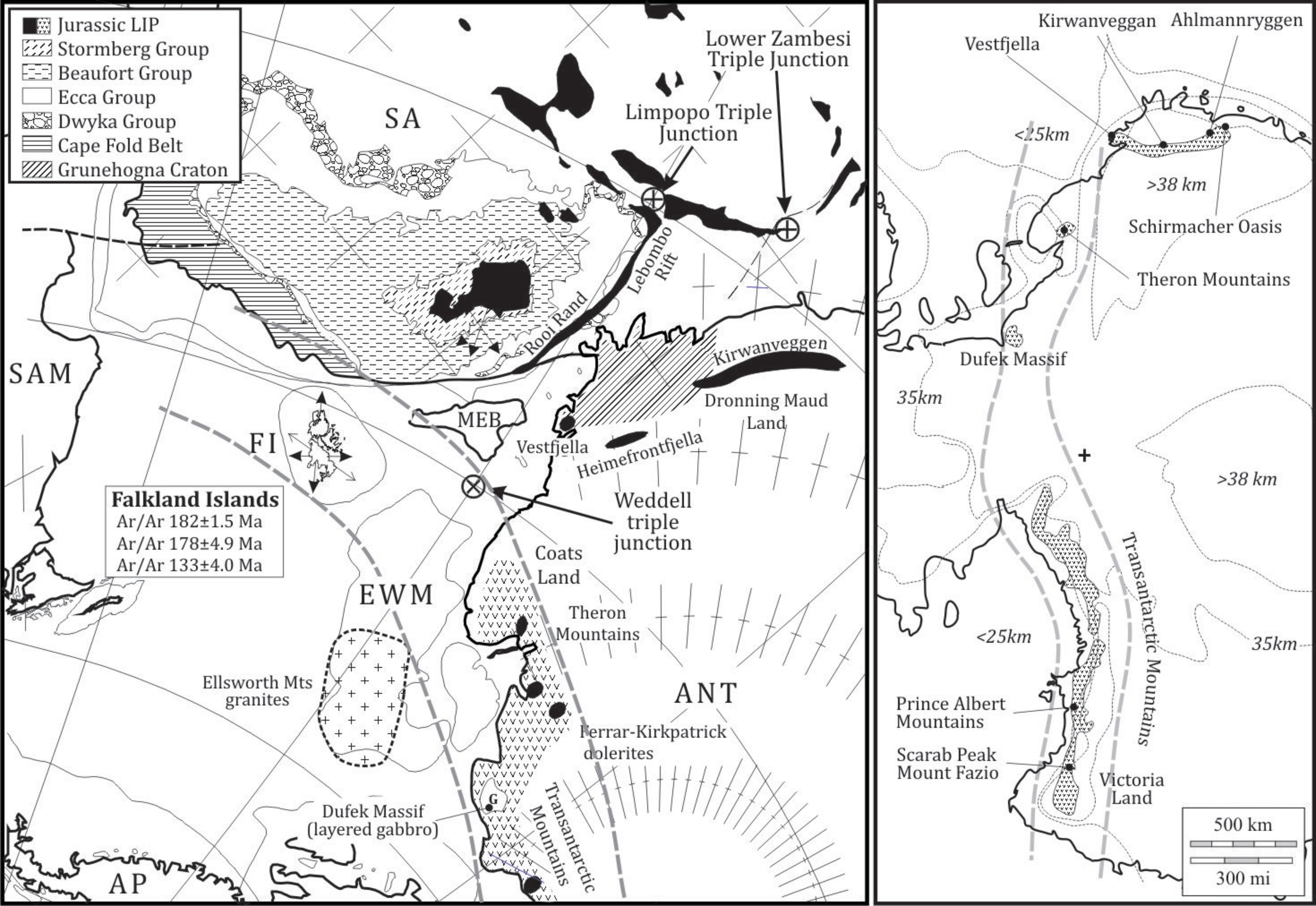

Jurassic LIP
Stormberg Group
Beaufort Group
Ecca Group
Dwyka Group
Cape Fold Belt
Grunehogna Craton
SA
SAM
FI
MEB
EWM
AP
ANT
Lower Zambesi Triple Junction
Limpopo Triple Junction
Lebombo Rift
Rooi Rand
Kirwanveggen
Dronning Maud Land
Vestfjella
Heimefrontfjella
Weddell triple junction
Coats Land
Theron Mountains
Falkland Islands
Ar/Ar 182±1.5 Ma
Ar/Ar 178±4.9 Ma
Ar/Ar 133±4.0 Ma
Ellsworth Mts granites
Ferrar-Kirkpatrick dolerites
Dufek Massif (layered gabbro)
G
Transantarctic Mountains
Kirwanveggen
Ahlmannryggen
Vestfjella
<25km
>38 km
Schirmacher Oasis
Theron Mountains
Dufek Massif
35km
>38 km
<25km
35km
Prince Albert Mountains
Scarab Peak Mount Fazio
Transantarctic Mountains
Victoria Land
500 km
300 mi

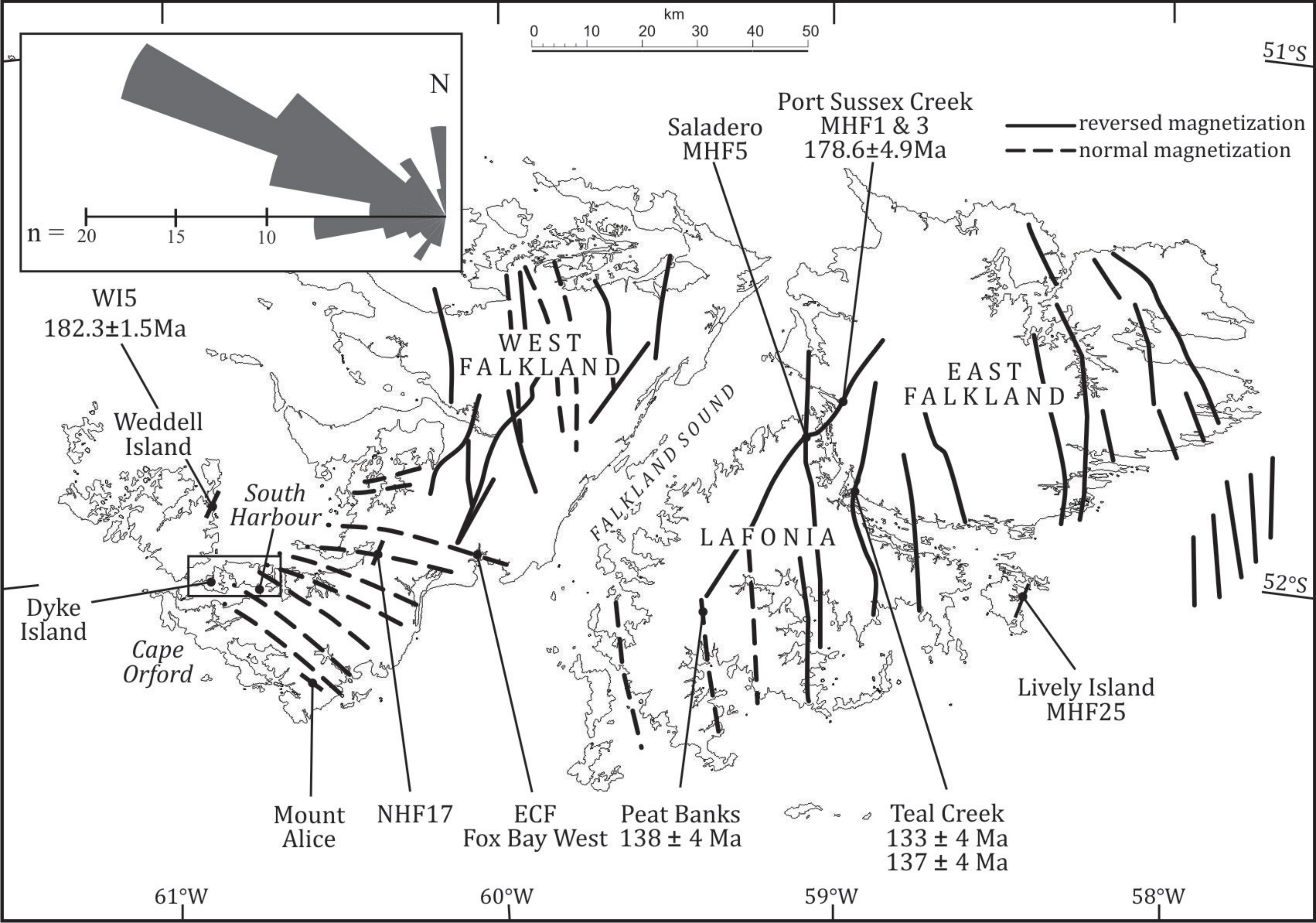

km
0 10 20 30 40 50
51°S
52°S
N
n = 20 15 10
Port Sussex Creek
MHF1 & 3
178.6±4.9Ma
Saladero
MHF5
reversed magnetization
normal magnetization
WI5
182.3±1.5Ma
WEST
FALKLAND
EAST
FALKLAND
FALKLAND SOUND
LAFONIA
Weddell
Island
South
Harbour
Dyke
Island
Cape
Orford
Lively Island
MHF25
Mount
Alice
NHF17
ECF
Fox Bay West
Peat Banks
138 ± 4 Ma
Teal Creek
133 ± 4 Ma
137 ± 4 Ma
61°W
60°W
59°W
58°W

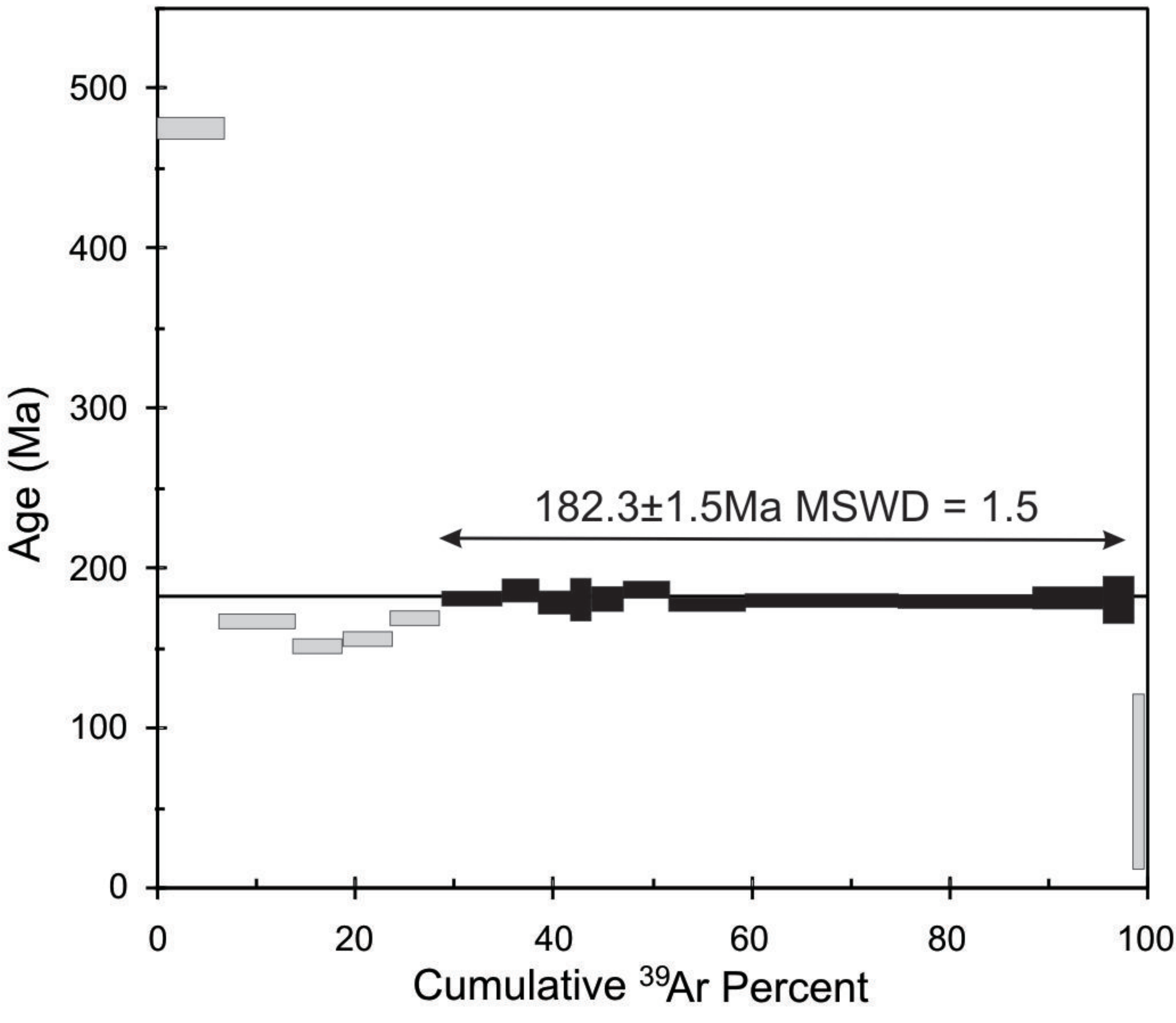

Age (Ma)
500
400
300
200
100
0
182.3±1.5Ma MSWD = 1.5
0
20
40
60
80
100
Cumulative 39Ar Percent

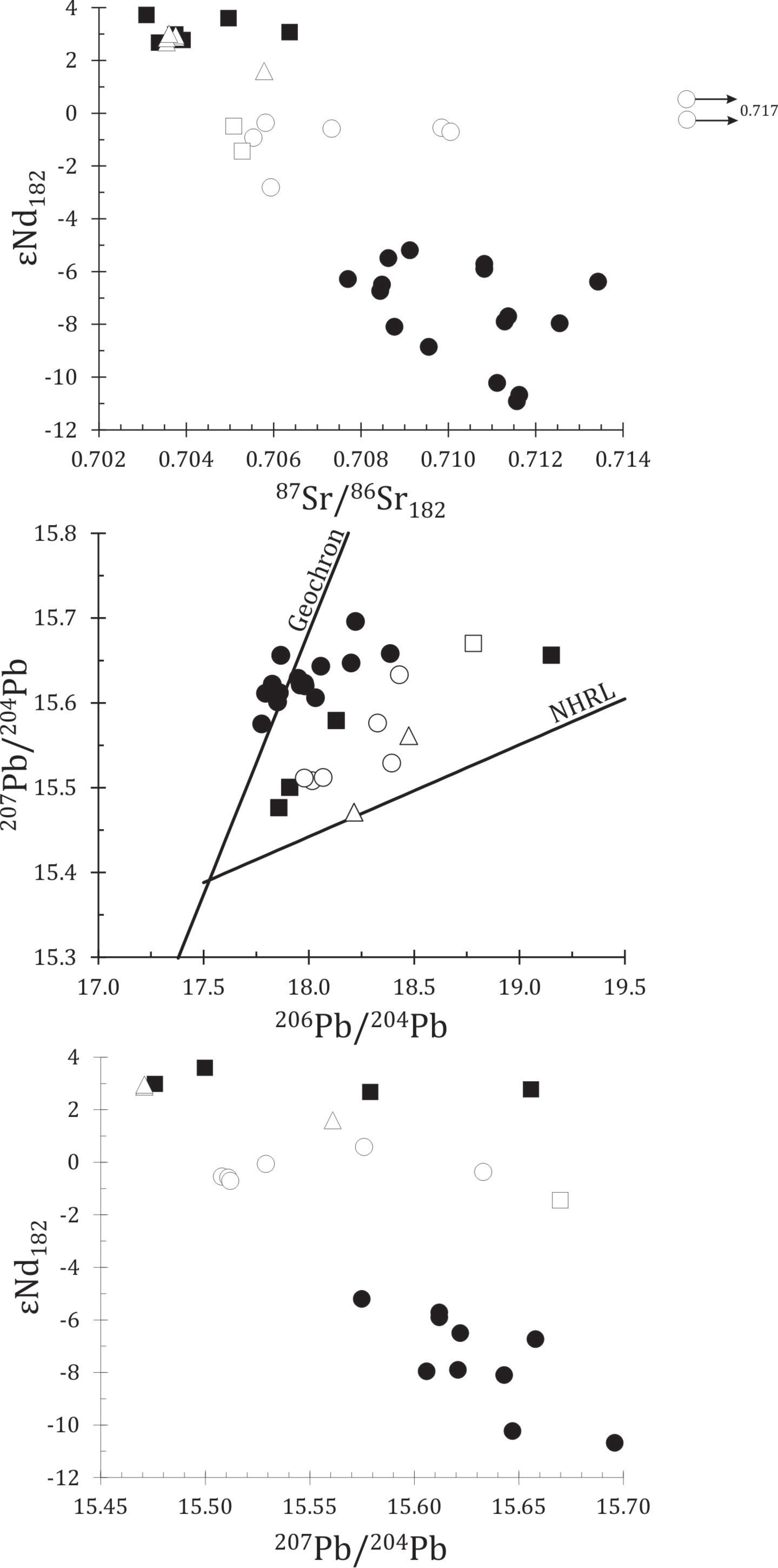

4
2
0
-2
-4
-6
-8
-10
-12
εNd182
0.702
0.704
0.706
0.708
0.710
0.712
0.714
87Sr/86Sr182
0.717
15.8
15.7
15.6
15.5
15.4
15.3
207Pb/204Pb
Geochron
NHRL
17.0
17.5
18.0
18.5
19.0
19.5
206Pb/204Pb
4
2
0
-2
-4
-6
-8
-10
-12
εNd182
15.45
15.50
15.55
15.60
15.65
15.70
207Pb/204Pb

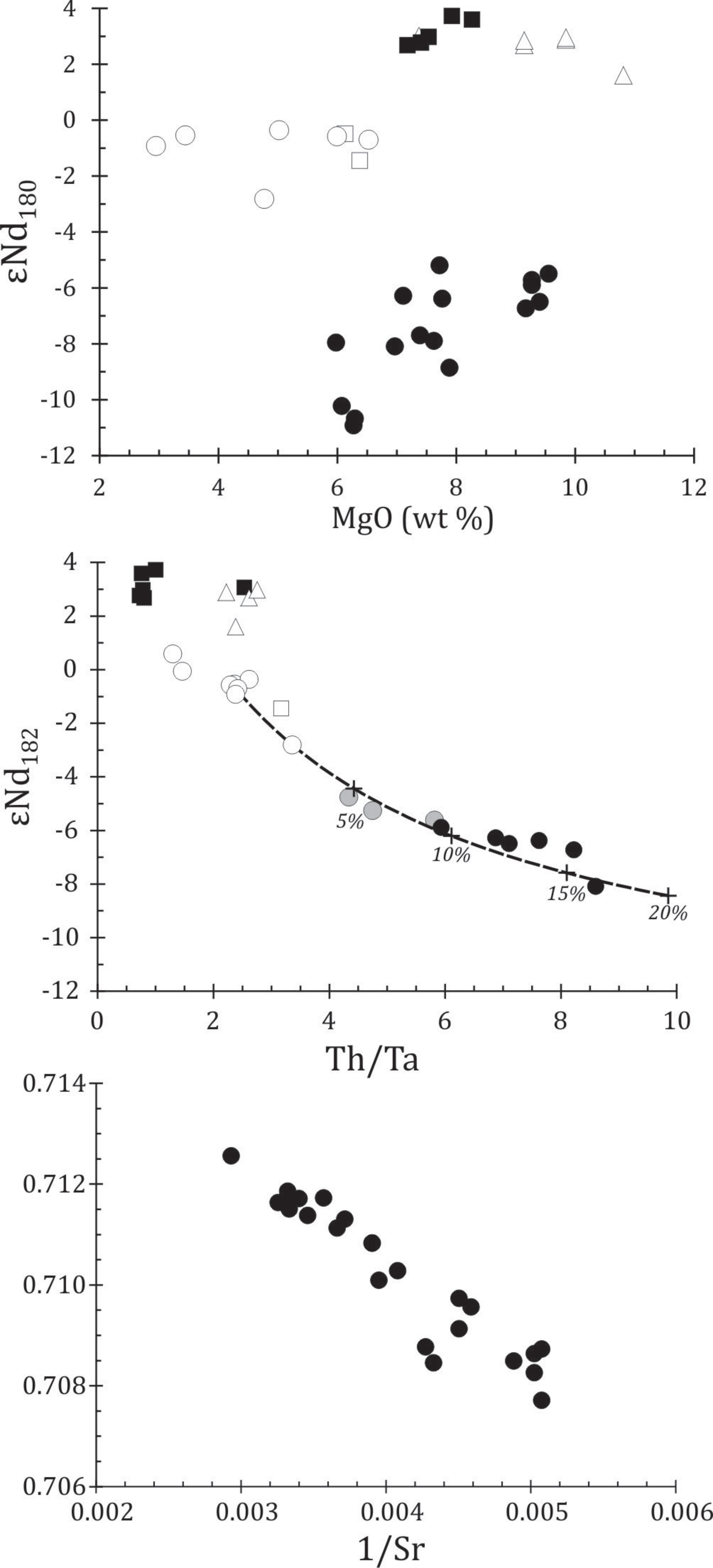

εNd180
MgO (wt %)
εNd182
5%
10%
15%
20%
Th/Ta
1/Sr

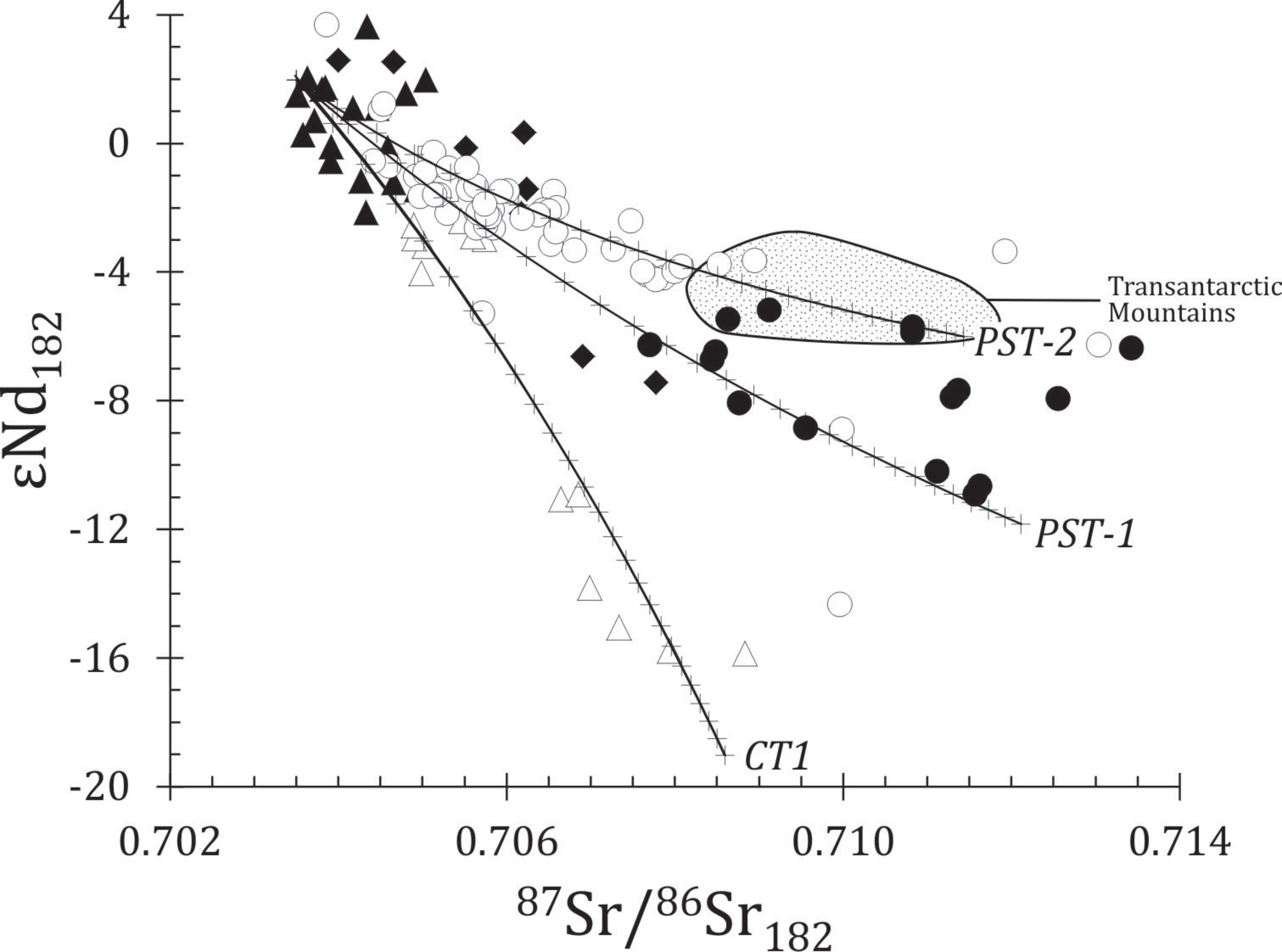

4
0
-4
-8
-12
-16
-20
εNd182
0.702
0.706
0.710
0.714
87Sr/86Sr182
Transantarctic Mountains
PST-2
PST-1
CT1

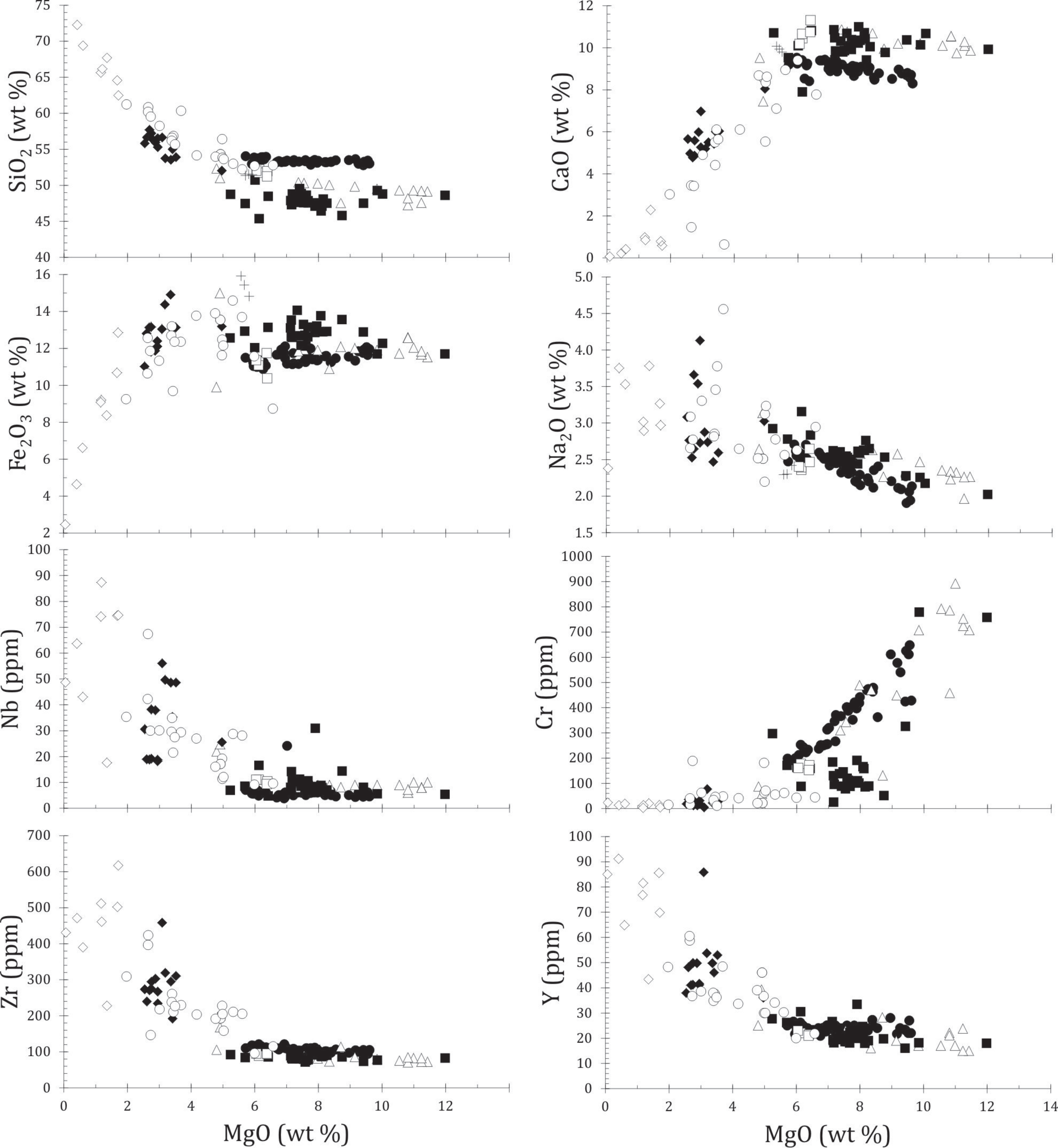

SiO_2 (wt %)
CaO (wt %)
Fe_2O_3 (wt %)
Na_2O (wt %)
Nb (ppm)
Cr (ppm)
Zr (ppm)
Y (ppm)
MgO (wt %)
MgO (wt %)

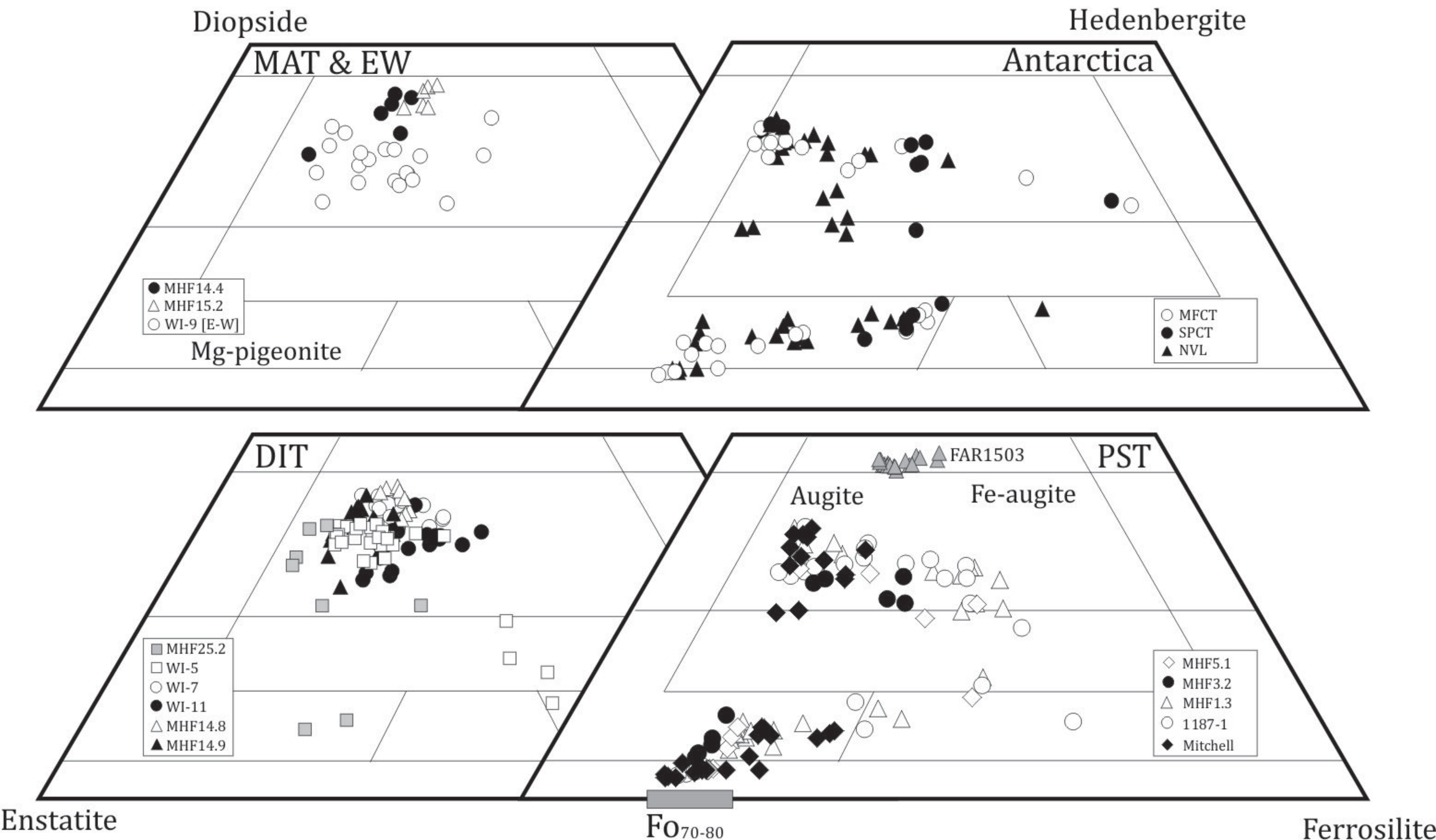

Diopside
Hedenbergite
MAT & EW
Antarctica
MHF14.4
MHF15.2
WI-9 [E-W]
Mg-pigeonite
MFCT
SPCT
NVL
DIT
PST
FAR1503
Augite
Fe-augite
MHF25.2
WI-5
WI-7
WI-11
MHF14.8
MHF14.9
MHF5.1
MHF3.2
MHF1.3
1187-1
Mitchell
Enstatite
Fo70-80
Ferrosilite

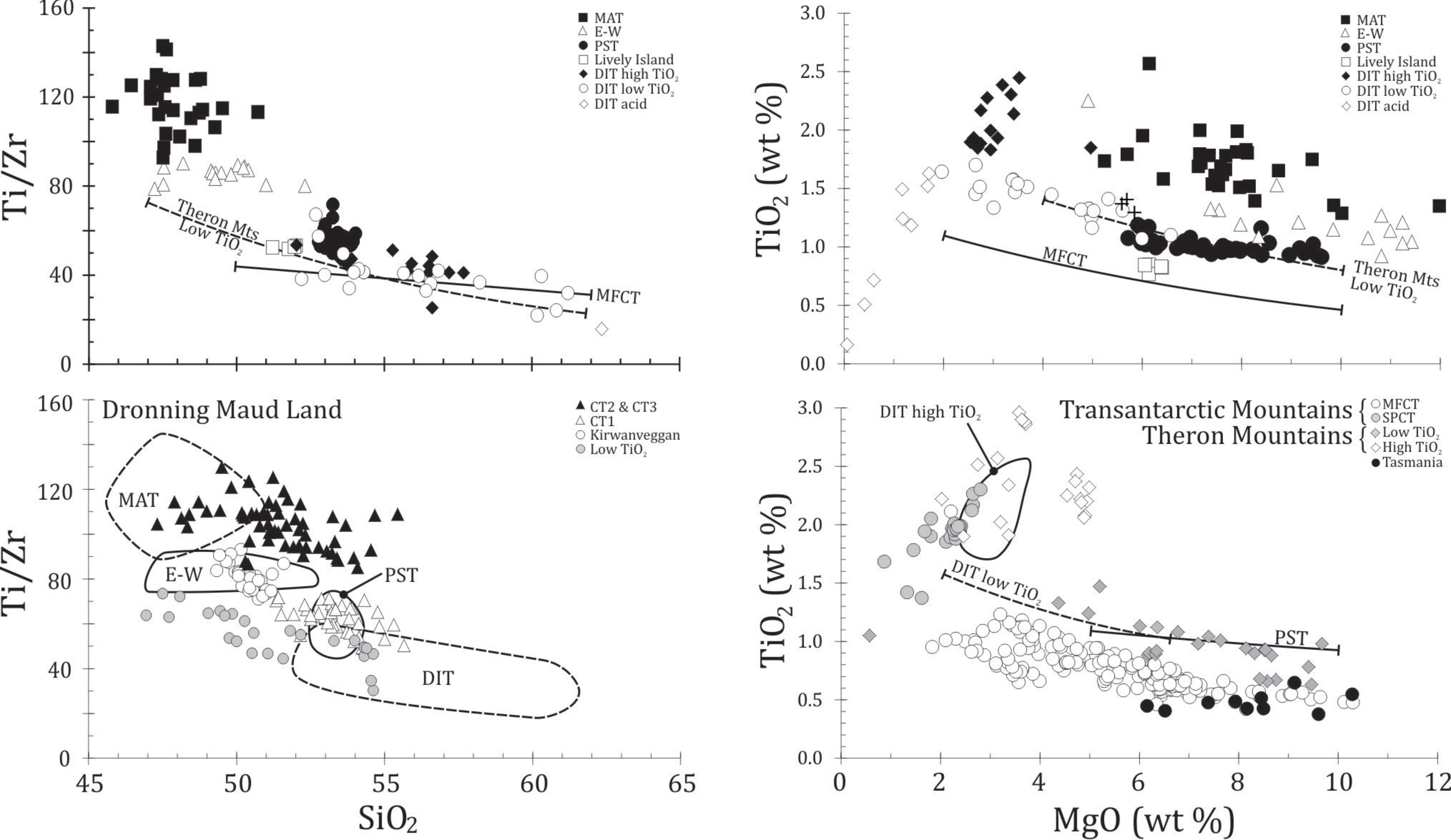

MAT
E-W
PST
Lively Island
DIT high TiO2
DIT low TiO2
DIT acid
Theron Mts Low TiO2
MFCT
Ti/Zr
TiO2 (wt %)
Dronning Maud Land
CT2 & CT3
CT1
Kirwanveggan
Low TiO2
MAT
E-W
PST
DIT
DIT high TiO2
DIT low TiO2
PST
Transantarctic Mountains
MFCT
SPCT
Theron Mountains
Low TiO2
High TiO2
Tasmania
SiO2
MgO (wt %)

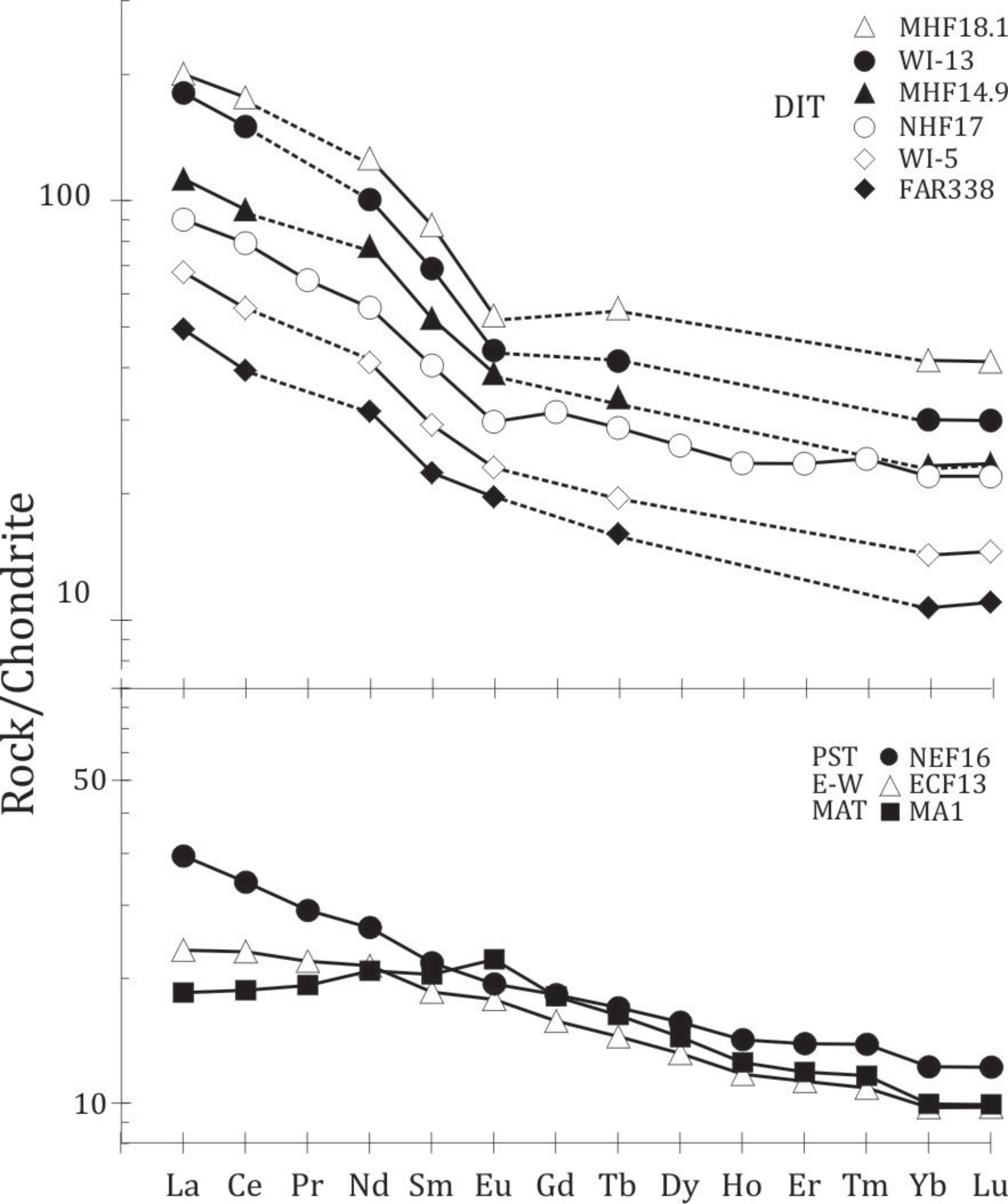
MHF18.1
WI-13
MHF14.9
NHF17
WI-5
FAR338
DIT
100
10
Rock/Chondrite
PST NEF16
E-W ECF13
MAT MA1
50
10
La
Ce
Pr
Nd
Sm
Eu
Gd
Tb
Dy
Ho
Er
Tm
Yb
Lu

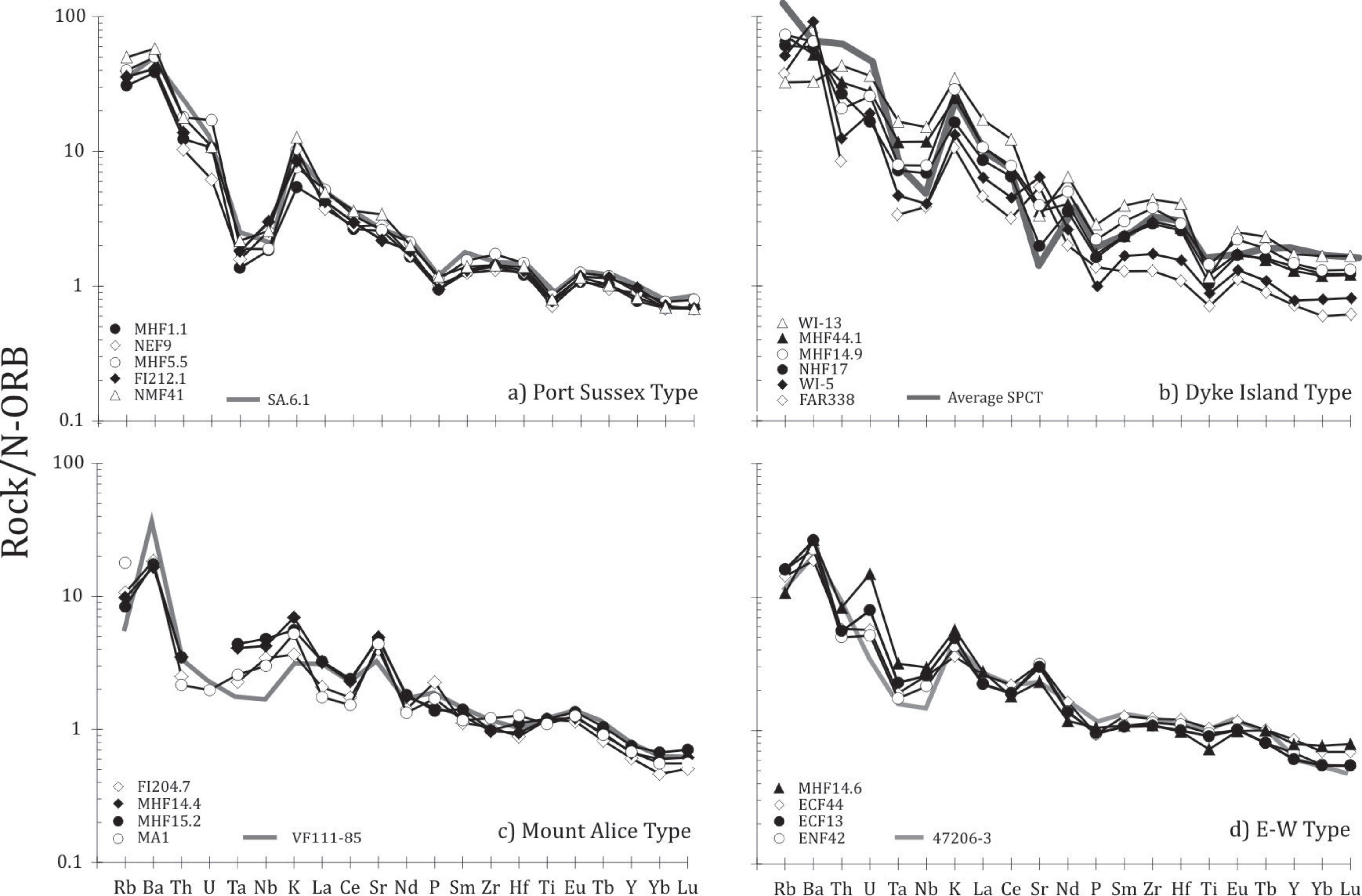
Rock/N-ORB
100
10
1
0.1
Rb Ba Th U Ta Nb K La Ce Sr Nd P Sm Zr Hf Ti Eu Tb Y Yb Lu
MHF1.1
NEF9
MHF5.5
FI212.1
NMF41
SA.6.1
a) Port Sussex Type
WI-13
MHF44.1
MHF14.9
NHF17
WI-5
FAR338
Average SPCT
b) Dyke Island Type
FI204.7
MHF14.4
MHF15.2
MA1
VF111-85
c) Mount Alice Type
MHF14.6
ECF44
ECF13
ENF42
47206-3
d) E-W Type

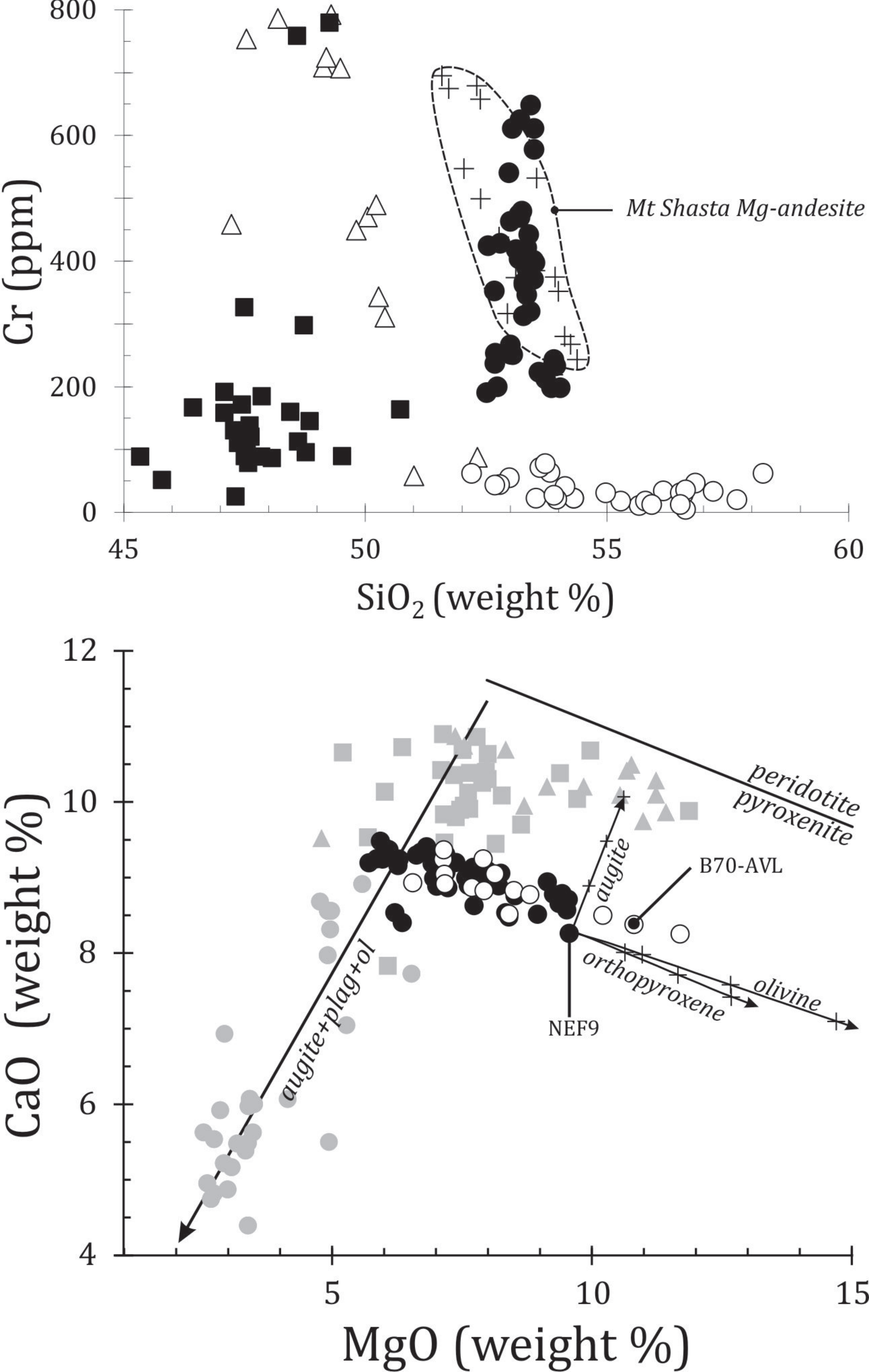

800
600
400
200
0
Cr (ppm)
Mt Shasta Mg-andesite
45
50
55
60
SiO2 (weight %)
12
10
8
6
4
CaO (weight %)
peridotite
pyroxenite
augite
B70-AVL
augite+plag+ol
orthopyroxene
olivine
NEF9
5
10
15
MgO (weight %)

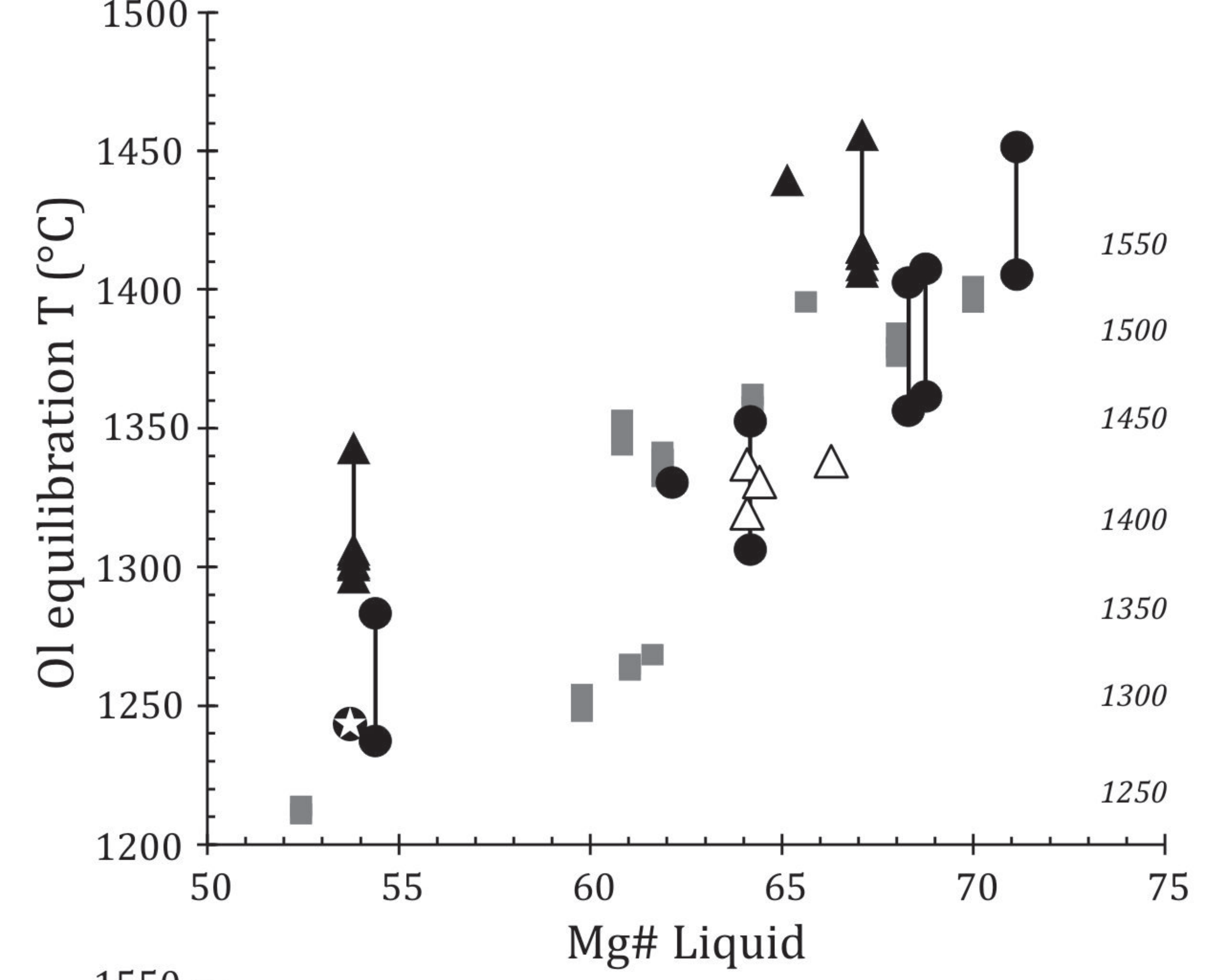
Ol equilibration T (°C)
Mg# Liquid
1550
1500
1450
1400
1350
1300
1250

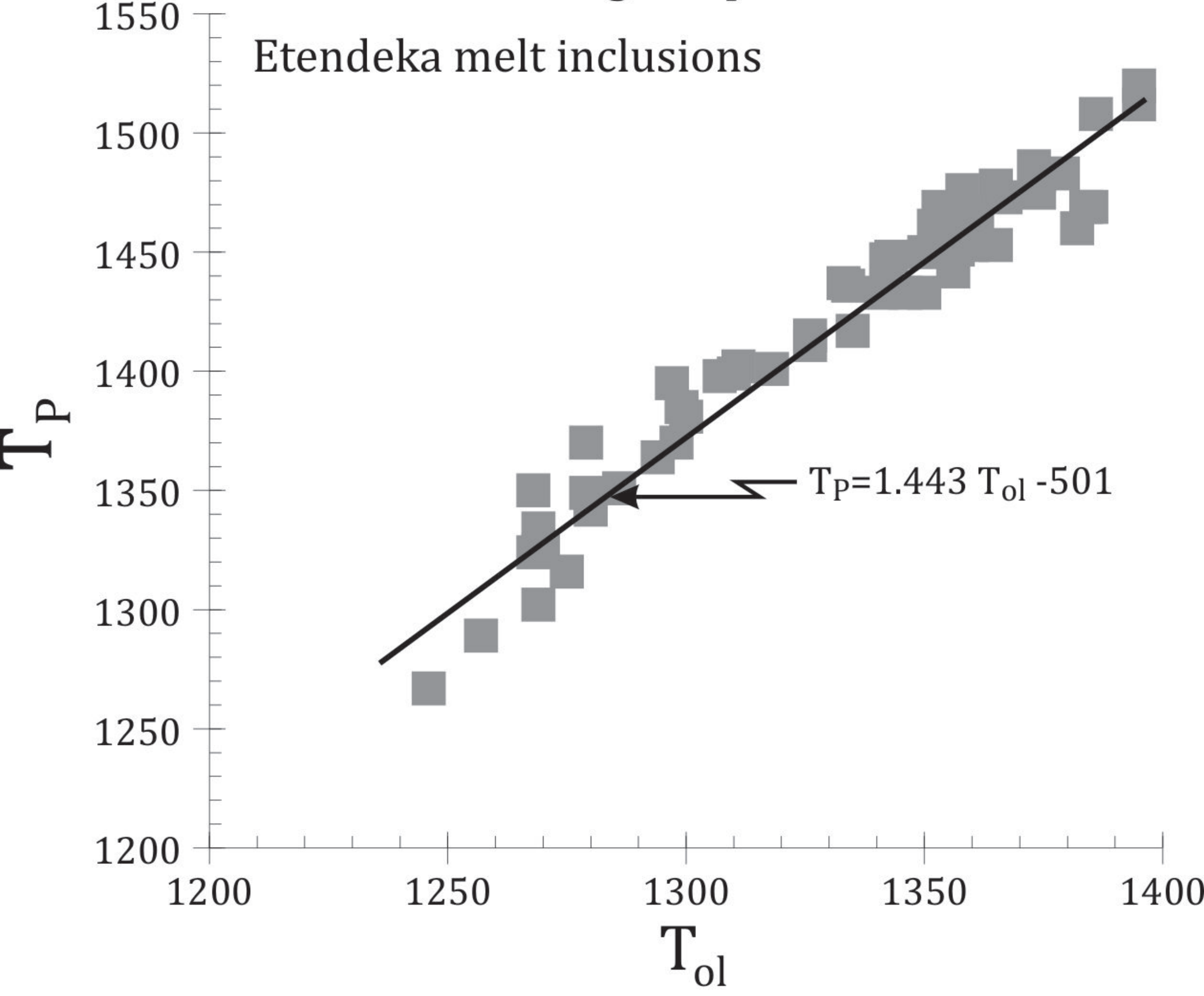
Etendeka melt inclusions
T_P=1.443 T_{ol} -501
T_P
T_{ol}

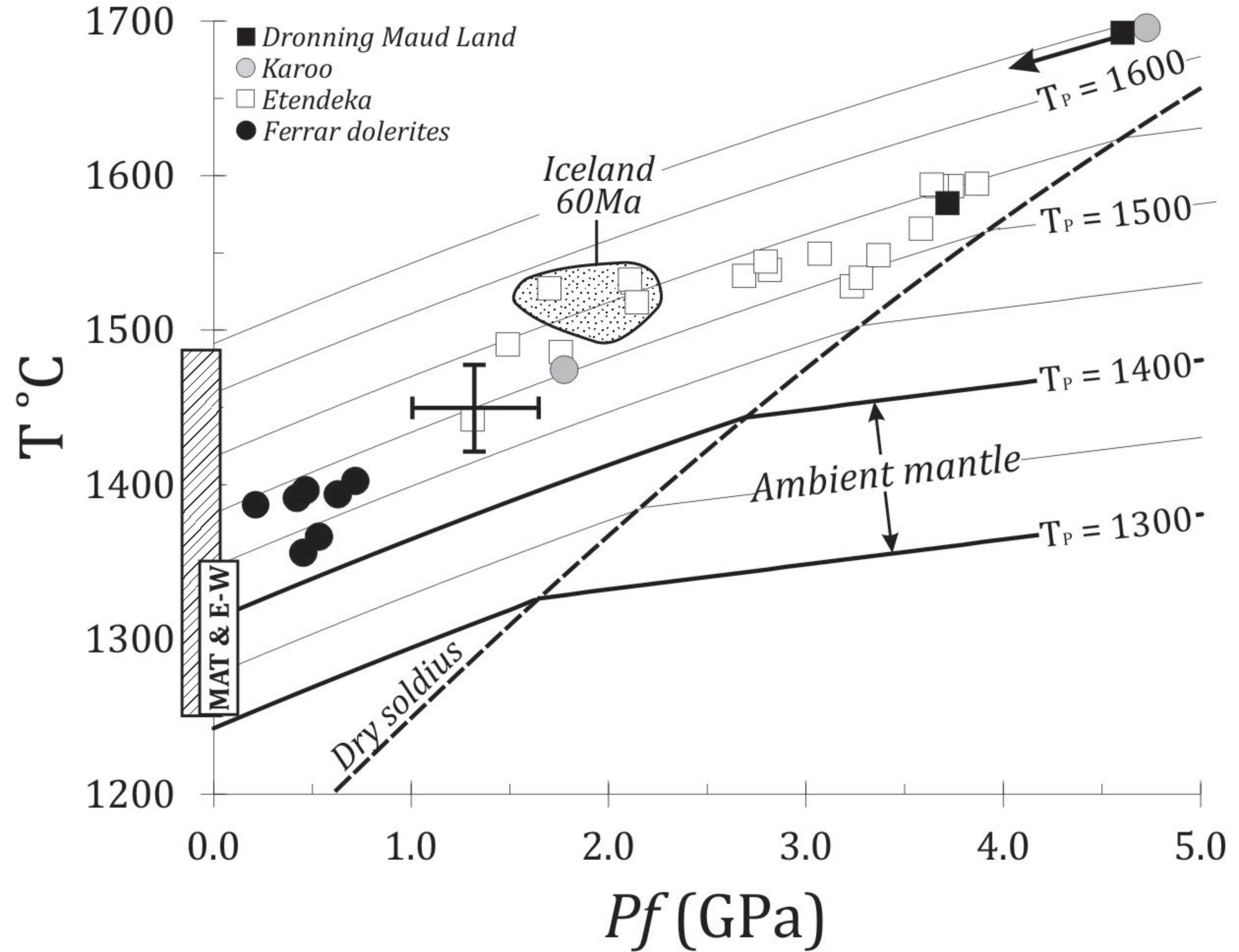
Dronning Maud Land
Karoo
Etendeka
Ferrar dolerites
Iceland 60Ma
T_P = 1600
T_P = 1500
T_P = 1400
T_P = 1300
Ambient mantle
MAT & E-W
Dry soldius
T °C
Pf (GPa)

Sample	MHF15.2	MHF14.4	MHF15.1	MA1	MHF41.3	MHF18.1	MHF44.1	MHF18.3	NHF17
	MAT	MAT	MAT	MAT	DIT Acid	DIT Acid	DIT Acid	DIT	DIT
SiO_2	45.92	47.40	48.56	47.51	68.92	64.11	55.49	53.24	53.97
TiO_2	1.81	1.52	1.71	1.39	0.71	1.51	1.54	1.30	1.32
Al_2O_3	15.70	16.39	16.71	16.45	15.03	15.96	15.28	15.01	13.27
Fe_2O_3	13.60	13.23	12.52	12.91	6.57	10.61	12.31	12.05	13.88
MnO	0.16	0.17	0.21	0.20	0.10	0.06	0.22	0.12	0.22
MgO	8.00	7.51	7.15	8.27	0.60	1.67	3.48	4.99	4.77
CaO	10.59	10.65	9.80	10.05	0.40	0.75	5.63	8.56	8.68
K_2O	2.59	2.53	2.53	2.65	3.51	3.25	3.76	3.21	2.52
P_2O_5	0.30	0.05	0.17	0.38	3.29	0.75	1.78	0.66	1.18
Na_2O	0.20	0.17	0.19	0.20	0.21	0.69	0.20	0.17	0.19
TOTAL	98.87	99.63	99.56		99.34	99.36	99.69	99.30	
Loss	1.5	1.90	2.25		3.44	3.30	1.56	3.64	
Rb	4.7	5.5	2.0	10	59.6	20.5	40	17.6	34
Sr	424	444	381	396	715	1204	324	367	178
Nb	11.2	9.9	10.7	7	72	74.4	27.4	12.0	16
Zr	80	79	80	90	620	502	226	158	192
Y	21.1	18.6	18.2	19	64.8	85.5	36.2	30.0	39
Cr	89	78	95	89	19	13	11	71	21
Ni	119	102	121	116	2.0	8	6	95	10
Ba	110	105	103	827	862	2939	528	199	371
La	8.1	8.0	7.9	4.37	68.9	47.5	27.0	15.7	21.36
Ce	18.0	17.2	18.3	11.45	140.0	108	55.6	32.6	48.50
Pr				1.83					6.14
Nd	13.3	12.8	13.8	9.73	69.3	58.9	29.7	20.5	25.93
Sm	3.72	3.32	3.78	3.08	13.60	13.2	6.18	5.32	6.12
Eu	1.38	1.25	1.42	1.29	3.41	3.09	1.77	1.63	1.72
Gd				3.72					6.46
Tb	0.7	0.63	0.72	0.61	2.06	2.07	1.04	0.94	1.07
Dy				3.66					6.62
Ho				0.71					1.34
Er				1.97					3.91
Tm				0.30					0.62
Yb	2.05	1.83	2.04	1.69	7.47	7.07	3.62	2.81	3.74
Lu	0.32	0.28	0.33	0.23	1.11	1.05	0.55	0.44	0.0.56
Th	0.42	0.42	0.48	0.26	6.54	5.6	3.90	1.49	3.19
U				0.09	2.10	2.2	1.30	0.9	0.77
Ta	0.58	0.54	0.6	0.3	4.47	4.32	1.54	0.57	0.95
Hf	2.28	1.94	2.26	2.60	13.80	11.7	5.53	3.78	5.29
Pb				1.07					13.83
Cs	0.3	0.35	0.2		0.20	0.3	0.38	0.4	
Co	48.2	42.60	49.3		7.40	12.5	29.4	50.6	
Sc	28.9	25.40	28.6		13.30	16.3	23.7	15.8	
$^{87}Sr/^{86}Sr$	0.70400	0.70385±1	0.70342		0.71745	0.71720	0.70730	0.70618	
± 2SE	±14	7	±15		±14	±17	± 17	±17	
$^{87}Sr/^{86}Sr_{182}$	0.70392	0.70375	0.70338	0.70497	0.7168	0.71716	0.70633	0.70581	0.70594
$^{143}Nd/^{144}Nd$	0.512747	0.512743	0.512738		0.512542	0.512595	0.512561	0.512572	
± 2SE	±6	±17	±6		±7	±7	± 6	±5	
$^{143}Nd/^{144}Nd_{182}$	0.512537	0.512548	0.512532	0.512588	0.512398	0.512427	0.512405	0.512377	0.512259
εNd_{190}	2.8	3.0	2.7	3.6	-0.1	0.6	0.1	-0.4	-2.8
$^{206}Pb/^{204}Pb$	19.152±6	17.858±7	18.131±7	17.91	18.393±6	18.326±8		18.430±8	
$^{207}Pb/^{204}Pb$	15.656±5	15.476±6	15.579±7	15.50	15.529±6	15.576±8		15.633±7	
$^{208}Pb/^{204}Pb$	38.464±13	37.425±18	37.762±16	37.57	37.583±12	37.880±20		37.944±2	

Sample	WI-5	MHF14.9	WI-3	1187-1	#1503	NEF9	NMF41	MHF1.1	MHF5.5
	DIT	DIT	DIT	PST	PST	PST	PST	PST	PST
SiO_2	52.44	56.06	60.88	52.67	53.20	52.41	53.59	53.49	53.01
TiO_2	1.10	1.81	1.63	0.97	1.02	0.89	1.02	0.99	1.07
Al_2O_3	19.53	14.30	15.24	14.00	12.90	15.69	14.87	13.15	13.90
Fe_2O_3	8.66	12.28	9.19	11.94	11.90	11.50	11.25	11.29	12.03
MnO	0.12	0.18	0.12	0.14	0.14	0.13	0.17	0.13	0.16
MgO	6.54	2.93	1.96	7.74	9.43	5.96	6.29	9.15	6.93
CaO	7.73	5.22	3.01	8.63	8.79	9.35	9.24	8.94	9.18
K_2O	2.92	4.10	5.74	2.45	1.90	2.61	2.52	2.10	2.52
P_2O_5	0.22	2.06	1.10	0.98	0.46	0.77	0.92	0.40	0.55
Na_2O	0.11	0.25	0.59	0.18	0.16	0.16	0.14	0.11	0.13
Total	99.36	99.20	99.45	99.70	99.90			99.75	99.48
Loss	3.28	4.12	2.81	1.50	0.50			1.26	2.62
Rb	29	40.8	18.2	33.1	14.2	22	28	17	22
Sr	582	358	302	533	205	256	307	232	234
Nb	9.5	18.2	35.2	5.8	4.9	6	6	4.3	4.4
Zr	115	267	309	110	93	97	106	104	113
Y	21.8	41.1	48.2	23.9	23.1	25	23	22	25.1
Cr	44	31	15	352	625	589	223	577	255
Ni	7	20	2.0	100	170	133	75	146	91
Ba	153	1409	207	nd	nd	1235	365	250	316
La	16.0	26.7	42.8	11.6	9.3	9.35	12.42	10.10	12.90
Ce	33.9	58.3	91.9	25.1	20.1	20.87	27.19	19.90	24.90
Pr						2.77	3.44		
Nd	19.2	36.4	47.0	14.7	12.3	12.37	14.64	12.00	15.3
Sm	4.41	7.92	10.4	3.58	3.15	3.29	3.68	3.34	4.06
Eu	1.34	2.25	2.55	1.22	1.05	1.12	1.19	1.09	1.28
Gd						3.76	4.16		
Tb	0.73	1.27	1.55	0.72	0.63	0.64	0.68	0.77	0.79
Dy						3.98	4.20		
Ho						0.80	0.83		
Er						2.30	2.37		
Tm						0.35	0.36		
Yb	2.43	3.97	5.11	2.14	1.93	2.08	2.12	2.09	2.33
Lu	0.37	0.60	0.76	0.33	0.28	0.31	0.31	0.32	0.36
Th	1.50	2.48	5.17	1.83	1.35	1.24	2.14	1.48	2.15
U	0.90	1.20	1.70	0.80	0.50	0.29	0.51	0.5	0.8
Ta	0.62	1.04	2.19	0.24	0.19	0.21	0.29	0.18	0.25
Hf	3.18	5.94	8.35	2.73	2.33	2.6	2.86	2.49	3.03
Pb						5.55	4.93		
Cs	0.28	0.56	0.20	0.42	0.29			2.24	0.74
Co	23.20	35.00	16.70	43.30	47.30			50.8	42.9
Sc	18.80	24.70	18.40	25.70	26.60			27.8	28.2
$^{87}Sr/^{86}Sr$	0.71042	0.70730	0.71029	0.71448	0.70900			0.70900	0.70948
± 2 SE	±6	± 17	± 23	±1	± 2			± 18	± 17
$^{87}Sr/^{86}Sr_{182}$	0.71004	0.7055	0.70983	0.71400	0.70846	0.71083		0.70842	0.70873
$^{143}Nd/^{144}Nd$	0.512533	0.512561	0.512535	0.512252	0.512255			0.512259	0.512181
± 2SE	±8	± 6	± 7	±7	± 0			± 6	± 6
$^{143}Nd/^{144}Nd_{182}$	0.51236	0.512349	0.512369	0.512069	0.512063	0.512367		0.51205	0.511981
εNd_{190}	-0.7	-0.9	-0.6	-6.4	-6.5	-5.7		-6.7	-8.1
$^{206}Pb/^{204}Pb$	18.067±9		18.016±10		17.826±11	17.86		18.394 ±8	18.057± 7
$^{207}Pb/^{204}Pb$	15.512±8		15.508±10		15.622 ±8	15.61		15.658± 8	15.643 ±8
$^{208}Pb/^{204}Pb$	37.425±12		37.492±26		38.044±19	37.97		38.143±20	38.246±16

Sample	ECF13	ECF42	ECF44	MHF14.6	MHF25.1
	EW	EW	EW	EW	Lively
SiO_2	49.49	49.82	50.40	47.02	51.76
TiO_2	1.15	1.21	1.32	0.92	0.82
Al_2O_3	14.30	14.47	15.22	14.79	15.94
Fe_2O_3	11.91	11.99	11.85	12.54	10.33
MnO	0.17	0.18	0.02	0.19	0.13
MgO	9.85	9.14	7.38	10.77	6.38
CaO	10.20	10.20	10.87	10.49	11.27
K_2O	2.47	2.58	2.57	2.33	2.46
P_2O_5	0.36	0.31	0.26	0.41	0.73
Na_2O	0.11	0.11	0.11	0.11	0.17
Total				99.57	99.63
Loss				2.20	1.88
Rb	9	9	8	6	10.9
Sr	269	282	283	208	231
Nb	6	5	6	6.9	10.3
Zr	80	85	91	81	93
Y	17	19	24	22.1	21.4
Cr	707	449	310	458	172
Ni	236	174	113	254	63
Ba	167	144	126	208	205
La	5.54	5.60	6.55	6.9	10.8
Ce	14.19	14.29	16.48	13.5	21.3
Pr	2.09	2.10	2.45		
Nd	10.01	10.16	11.95	8.6	11.9
Sm	2.80	2.84	3.37	2.87	2.9
Eu	1.03	1.03	1.20	1.01	0.92
Gd	3.25	3.29	4.10		
Tb	0.54	0.54	0.68	0.67	0.61
Dy	3.35	3.35	4.42		
Ho	0.66	0.67	0.85		
Er	1.87	1.90	2.41		
Tm	0.28	0.28	0.36		
Yb	1.66	1.68	2.11	2.34	2.41
Lu	0.25	0.25	0.31	0.36	0.4
Th	0.67	0.60	0.69	1.0	1.68
U	0.37	0.24	0.27	0.7	0.8
Ta	0.30	0.23	0.25	0.42	0.53
Hf	2.05	2.27	2.48	2.01	2.32
Pb	2.19	2.65	2.65		
Cs				0.3	0.47
Co				61.4	39.3
Sc				35	37.4
$^{87}Sr/^{86}Sr$				0.70600	0.70564
± 2 SE				±2	±15
$^{87}Sr/^{86}Sr_{182}$	0.70579	0.70376	0.70355	0.70578	0.70527
$^{143}Nd/^{144}Nd$				0.512726	0.512505
± 2SE				±7	±8
$^{143}Nd/^{144}Nd_{182}$	0.512561	0.512551	0.512565	0.512475	0.512322
εNd_{190}	2.9	2.7	3.0	1.6	-1.5
$^{206}Pb/^{204}Pb$		18.21		18.474±7	18.781± 9
$^{207}Pb/^{204}Pb$		15.47		15.561±8	15.670±9
$^{208}Pb/^{204}Pb$		37.58		38.111±15	38.300±23

Table 2. Geochemical, mineralogical and petrographical characteristics of the different groups of Falkland Islands intrusions.

Type	**Type locality**	**Mitchell[1]**	**Stone[2]**	**Petrographic features**	**Mineralogy**	**Subgroup**	**Mg#**	**SiO_2**	**TiO_2**	**Ti/Zr**	**Zr/Y**	**$^{87}Sr/^{86}Sr_{182}$**	**εNd_{182}**
Dyke Island (DIT)	Dyke Island 51º59'33" S 60º52'50" W	Not defined	Radial swarm	Fine-grained aphyric, rarely plagioclase ± augite-phyric	Plag + Aug	Acid	<22	62-75	0.2-1.6	<31	5.0-8.8	0.7055-0.7098	-2.8 to -0.5
						Low TiO_2	27-57	52-61	1.1-1.7	24-67	4.8-7.4		
						High TiO_2	41-51	53-58	>1.80	25-53	6.8-8.4		
Port Sussex Creek (PST)	Port Sussex 51º40'15" S 58º58'41" W	N-S	NE-SW	Coarse-grained dolerite	Pig ± Opx + Aug Rare Ol + Di	none	48-58	52-54	0.9-1.2	50-70	3.6-5.3	0.7077 -0.7134	-5.5 to -10.9
E-W	Fox Bay West 51º57'02" S 60º05'21" W	E-W	E-W	Coarse-grained olivine dolerite	Ol + Plag ± Aug	none	42-64	47-54	1.0-1.9	77-90	3.2-4.8	0.7036-0.7058	-0.4 to +3.0
Mount Alice (MAT)	Mount Alice 52º09'12" S 60º35'55" W	Mount Alice	Radial swarm	Fine-grained plagioclase ± olivine phyric	Ol + Plag ± Aug	none	44-64	47-50	1.3-1.9	98-142	3.2-5.2	0.7031-0.7039	0.0 to +3.7
Lively Island (LI)	Lively Island 52º00'00" S 58º27'47" W	Lively Island	NE-SW	Coarse-grained with accessory biotite	Rare pigeonite	none	48-52	51-52	0.8-0.9	53	4.0-4.54	0.7053	-0.5 to -1.4

1. Groups described by Mitchell *et al*. (1999); 2. Groups defined by Stone *et al.* (2009)

Calculated extract for fractionation of PST and E-W intrusions

		PST		**E-W**		
	NGF16	MHF5.1	Calc	ECF12	ECF44	Calc
SiO_2	54.01	53.81	53.82	49.69	51.03	50.98
TiO_2	0.94	1.00	1.13	1.05	1.21	1.36
Al_2O_3	13.20	14.97	15.02	13.30	15.21	15.20
FeO	10.60	10.62	10.60	10.51	11.11	11.06
MnO	0.20	0.17	0.18	0.17	0.17	0.21
MgO	9.67	6.78	6.78	11.62	6.71	6.70
CaO	8.81	9.50	9.49	9.81	11.51	11.50
Na_2O	1.96	2.62	2.56	2.29	2.56	2.46
K_2O	0.48	0.42	0.56	0.32	0.39	0.39
P_2O_5	0.12	0.11	0.15	0.11	0.11	0.13
Extract			%			%
Olivine	Fo_{83}		0.0			57.0
Plagioclase	An_{70}		18.9			40.4
Orthopyroxene	$En_{71}Fs_{19}Wo_9$		74.7			
Clinopyroxene	$En_{51}Fs_{13}Wo_{33}$		6.4			2.6
Σ residuals^2			0.127			0.038
F			0.79			0.75

Table 4 AFC parameters for the trajectories shown in Fig. 12. R is the ratio of assimilated rock to crystal cumulate. A value appropriate for upper-crustal contamination has been used. F is the total amount of crystallization required to reach the most extreme composition on a particular trajectory. T_{CHUR} is the Chondritic Uniform Reservoir model Nd age for the most extreme composition on a particular trajectory, in Ga.

		AFC parameters								T_{CHUR}
		Sr	**Nd**	**εNd**	**$^{87}Sr/^{86}Sr$**	D_{Sr}	D_{Nd}	**R**	**F**	**(Ga)**
CT1	Source	50	5	2	0.7035	0.5	0.1	0.40	≤0.2	3.0
	Crust	400	20	-50	0.7120					
PST-1	Source	60	4	2	0.7035	0.5	0.1	0.40	≤0.2	2.2
	Crust	350	40	-20	0.7200					
PST-2	Source	100	5	2	0.7035	0.5	0.1	0.40	≤0.2	1.8
	Crust	350	60	-10	0.7250					